Role of the global oceans and land-atmosphere interaction on summertime interdecadal variability over northern Argentina

Marcelo Barreiro, Nicolas Díaz and Madeleine Renom

Unidad de Ciencias de la Atmósfera, Facultad de Ciencias
Universidad de la República, Uruguay

Revised: December 23rd, 2013

Corresponding author address:
Marcelo Barreiro
Unidad de Ciencias de la Atmósfera, Instituto de Física,
Facultad de Ciencias, Universidad de la República,
Igua 4225, Montevideo 11400, Uruguay.
Phone: +598 25258624
Fax: +598 25250580

Keywords: northern Argentina; interdecadal; rainfall variability; land-atmosphere interaction; predictability.

Abstract

This study uses experiments with an Atmospheric General Circulation Model (AGCM) to address the role of the oceans and the effect of land-atmosphere coupling on the predictability of summertime rainfall over northern Argentina focusing on interdecadal time scales during 1901-2006. Ensembles of experiments where the AGCM is forced with historical SST in the global, Pacific and tropical-north Atlantic domains are used. The role of land-atmosphere interaction is assessed comparing the output of simulations with active and climatological soil moisture.

A Maximum Covariance Analysis between precipitation and SST reveals the impact of the Pacific Decadal Oscillation, the Atlantic Multidecadal Oscillation and the equatorial-tropical south Atlantic on rainfall over northern Argentina. Model simulations further show that while the dominant influence comes from the Pacific basin, the Atlantic influence can explain a large transition from dry to wet decades over northern Argentina during the beginning of the 1970s. Analysis of anomalies before and after the transition reveals an upper level anticyclonic circulation off the Patagonian coast with barotropic structure. This circulation enhances the moisture transport and convergence in northern Argentina and, together with enhanced evaporation, increased the rainfall after 1970. The SST pattern is dominated by cold conditions in the equatorial Atlantic and warm eastern Pacific and south Atlantic.

We also found that land-atmosphere interaction leads to a representation of the long term rainfall evolution over northern Argentina that is closer to the observed one. Moreover, it leads to a smaller dispersion among ensemble members, thus resulting in a larger signal-to-noise ratio.

1. Introduction

Subtropical South America, defined loosely between 20ºS and 40ºS and to the east of the Andes is a region with large gradients in precipitation during the year. In summertime, the season characterized by the South American Monsoon System, it rains rather uniformly in the whole region although in larger amounts in the northeastern sector due to the presence of the South Atlantic Convergence Zone (SACZ). On the contrary, in austral winter there is a strong west-east rainfall gradient so that rainfall is very limited to the west of 60ºW and has a maximum next to the coast in southern Brazil and Uruguay. The subtropics are strongly influenced by El Niño-Southern Oscillation (ENSO) during most of the seasons with largest rainfall anomalies during southern springtime (e.g. Pisciottano et al 1994; Grimm et al 2000; Cazes et al 2003). Thus, most of the interannual predictability of rainfall is thought to come from the equatorial Pacific. Mechanisms through which ENSO influences subtropical South America include (1) direct effects through wave propagation from Rossby wave sources induced by anomalous latent heating and increased northerly moisture fluxes from the Amazon (e.g. Grimm et al 2000; Silvestri 2004; Grimm and Ambrizzi 2009), (2) indirect effects in which the atmospheric anomalies induced by El Niño change surface ocean conditions off south Brazil which then alter the persistence of atmospheric anomalies in this region (Barreiro 2010), and (3) indirect surface-atmosphere interaction effects by which the soil moisture anomalies in central-east Brazil and SST anomalies off the southeast Brazil coast produced in spring alter the precipitation anomalies in summer (Grimm et al. 2007).

The variability and predictability on longer, interdecadal, time scales is much less well known and has attracted interest only in recent years. Kayano and Andreoli (2007) show that the

Pacific Decadal Oscillation (PDO) influences the El Niño teleconnection over South America during the warm season such that rainfall anomalies are strongest when the positive (negative) phase of the PDO and El Niño (La Niña) coincide (also Andreoli and Kayano 2005). Consistently, other studies showed that the predictability of rainfall and air surface temperature over southeastern South America is different before and after the mid-1970s largely due to changes in the ENSO remote influence (e.g. Boulanger et al 2005, Antico 2008, Barreiro 2010). Recently, Renom et al (2011) found that changes in El Niño evolution after 1976 may have played a role in altering the relationship between temperature extreme events in Uruguay and the atmospheric circulation. Moreover, several authors have found that the ENSO rainfall signal on subtropical South America can be modulated by sea surface temperature (SST) anomalies in the tropical Atlantic and Indian oceans, which can thus induce low frequency variability (Barreiro and Tippmann 2008; Chan et al 2008; Mo and Berbery 2011; Taschetto and Ambrizzi 2012).

On 20-30 years time scale low frequency internal climate variability will superimpose on the observed long term trend (see for example Seager et al 2010) and it is therefore of much interest to understand the sources of this variability. In an attempt to address this issue, Seager et al (2010) claim that the tropical Atlantic SST anomalies associated with the Atlantic Multidecadal Oscillation (AMO) play a dominant role on low-frequency variability such that cold conditions there promote wet conditions over southeastern South America. They further suggest that the wetting trend of the last decades in this region is not related to anthropogenic radiative forcing but, instead, is mainly due to the influence of the AMO. Recently, Gonzalez et al (2013) have proposed that the stratospheric ozone depletion has also significantly contributed to the wetting trend over southeastern South America during 1960-1999, through a poleward displacement of the extratropical westerly jet. These latter results have important implications because the economy of a large portion of subtropical South America strongly depends on climate through hydroelectric production and agricultural activities. For example, the western Pampas in northern Argentina is particularly important for agriculture and in the last few decades of the 20th century the area of soybean production in this region expanded due to an increase in mean rainfall that has allowed crop production in areas that were traditionally used for livestock production (Baldi and Paruelo 2008; Magrin et al 2005). This region also hosts Laguna Mar Chiquita, the largest saline lake in South America that has shown large interdecadal variability during the 20th century most of it of natural (as opposed to anthropogenically forced) origin (Troin et al 2010).

In recent years it has become evident that once the oceanically-forced signal arrives over a certain continental region the atmospheric anomalies will be modified by the interaction with the surface (Koster et al., 2000, 2004), particularly during summertime. South America is one of those regions where the interaction between soil moisture and precipitation is important to correctly simulate the climatological fields and the South American Monsoon (Xue et al., 2006; Collini et al., 2008; Misra 2008; Ma et al., 2010, Sorensson and Menendez 2010). The observation that on interannual time scales precipitation anomalies in central-east Brazil during peak summer is negatively correlated with soil moisture in the previous spring, led Grimm et al (2007) to propose a feedback between the surface and the atmosphere to explain this relationship. Recently, Barreiro and Diaz (2011) have shown that the use of interactive soil moisture is of fundamental importance in simulating the right air surface temperature response and a strong positive rainfall signal during El Niño in summertime over southeastern South

America.

The aim of this study is to further explore the predictability of summertime rainfall over subtropical South America independent of the interannual ENSO signal. Specifically, the study is designed (1) to identify the role of the Atlantic and Pacific oceans in influencing rainfall on interdecadal time scales (e.g. can the Pacific explain all the variability?), and (2) to find out the role of land-atmosphere interaction on long time scales. To do so we analyze the covariant modes of variability between SST and rainfall with time series that show interdecadal time scales. Given our interest in long term climate variability and the disparity in the spatial distribution of rain gauges in South America we focus on northern Argentina (see Figure 1). This region has the best observational coverage over the whole XX century and has been shown to present interdecadal changes in summertime rainfall (e.g. Castañeda and Barros 2001, Boulanger et al 2005). Focusing on this region, we show that on long time scales both the Pacific and Atlantic oceans contribute to set up the right circulation anomalies that lead to rainfall variability in that area, suggesting the existence of interdecadal potential predictability. Furthermore, land-atmosphere coupling is shown to be important to correctly simulate the long term behavior in rainfall and increases the signal-to-noise ratio.

In the following section we describe the data sets used and model simulations performed to address the objectives of the study. In sections 3, 4 and 5 we describe the results concerning the role of the oceans on long term rainfall variability, while in section 6 we assess the role of the soil moisture feedback. The last section summarizes the main findings.

2. Data and model simulations

To address the objectives of the study we use observed data, as well as the output of experiments performed with an Atmospheric General Circulation Model (AGCM).

2.1 Observations

The observed precipitation field is taken from the Global Precipitation Climatology Centre (GPCC) Full Data Reanalysis V 4. The data is on a 1ºx1º grid in the period 1901-2006 (Schneider et al 2008). Before analysis the GPCC data was interpolated to the same grid of the AGCM. Rainfall products for South America face the problem of sparse information at the beginning of the last century, and the GPCC is no exception. Figure 1 shows the summertime (January-March, hereafter JFM) climatological precipitation during the period 1901-2006. This is the peak season of the South American Monsoon System and it rains over most of the continent. There is a maximum in the Amazon region that extends southeastward indicating the presence of the South Atlantic Convergence Zone. South of 20°S, in the subtropics, mean rainfall varies from 6 to 0.5 mm/day with a southwest-northeast gradient. In this study we will focus on northern Argentina which we define roughly by [40°S-26°S,68°W-60°W] (see Figure 1). The historical data coverage in northern Argentina has varied over the century: in 1901 there were about 25 gauges reporting data, increases rapidly to 45 gauges in 1920 and reaches a peak near the '70s with about 65 gauges in the area (Figure 2). In the following years there was a decline in the number of gauges so that in 2006 there are about as many gauges as there were in the 1920s. The spatial distribution of the average number of gauges per grid during the different decades shows that northern Argentina is the area with best coverage during the whole century (Figure 3). The coverage is better on the eastern portion and more sparse on the western region, even though since 1930s the coverage has improved in the latter. The maximum coverage during 1961-1980 as well as the decrease in coverage in the later decades can be clearly seen. Other areas like southeastern Brazil have increased enormously the number of reporting gauges over the last 50 years, but had only very limited coverage in the first part of the 20th century. Changes in the number of reporting gauges are a major source of data inhomogeneity during the century not only over this region, but over the whole South American continent. Even in the second half of the 20th century, a period that is considered to have much better coverage than the beginning of the century, there is a clear change in the number of rainfall gauges (Fuchs et al 2009). There is no easy way to deal with this problem, it is a reality we have to face in order to study long term climate variability in South America and has to be taken into account when interpreting the results.

To compare results we use the CRU TS v3.10 (Climate Research Unit, University of East Anglia) observational product (Harris et al 2012). The original resolution of this data set is 0.5°x0.5° and spans the same time period 1901-2006 but, as for GPCC, the CRU data was also interpolated to the same grid of the AGCM. Analyses were repeated using the CRU precipitation and, even though there are small differences, the main results of the study remain unaltered.

We also used rainfall and other atmospheric fields from 3 reanalysis products to try to validate the model simulation: NCEP-CDAS1 over the time period 1949-2006 with an original resolution of 1.875°x1.875° (Kalnay et al 1996), ERA40 from September 1957 to August 2002 with an original resolution of 2.5°x2.5° (Uppala et al 2005) and the 20th Century Reanalysis (V2) within 1901-2006 with an original resolution of 2°x2° (Compo et al 2011). All reanalysis products were interpolated from their original grids to the model resolution previous to analysis.

2.2 Model and experimental setup

The model used in this study is the AGCM from the International Centre for Theoretical Physics (ICTP AGCM), a full atmospheric model with simplified physics and a horizontal resolution of T30 (3.75°x3.75°) with 8 vertical levels (Kucharski et al 2005). The model is forced with historical global sea surface temperatures taken from the second version of the Extended Reconstructed Sea Surface Temperature data set (ERSSTv.2, Smith and Reynolds 2004). We note that the model has a bias consisting in weak summertime precipitation over southern Brazil and Uruguay thus having a relative maximum at about 60ºW instead of the southwest-northeast gradient observed in the subtropics east of the Andes (Kucharski et al 2005).

We performed four experiments that allow to assess the impacts of the Pacific and Atlantic oceans and to test the role of the land-atmosphere interaction. In the first experiment the model is forced with global historical SST (Global Ocean Global Atmosphere, hereafter called GOGA-AL). In the second experiment the model is forced with historical SST prescribed only in the Pacific ocean between 55ºS and 40ºN; elsewhere, SST climatology is prescribed (Pacific Ocean Global Atmosphere, hereafter called POGA-AL). A third experiment was run with prescribed historical SST only in the Atlantic basin north of 20ºS; elsewhere, SST climatology is prescribed (hereafter NAOGA-AL). Comparison among these experiments allows to separate the contributions of individual ocean basins. In all these experiments the AGCM is coupled to a land surface model to allow atmosphere-land interaction. The land surface model assumes a single soil layer with different depths for the energy and water balance and is described in Zeng et al (2000). In order to test the role of active soil moisture, we performed a final experiment where the AGCM is forced with global historical SST but has fixed soil moisture to its climatological value (hereafter called GOGA). In all experiments the AGCM was integrated from 1880 to 2006, starting from 9 different initial atmospheric conditions in order to create a 9-member ensemble for each experiment. In this study we only consider the period 1901-2006, as for observations, and anomalies are calculated with respect to that period.

As shown in Figure 4 the AGCM forced with historical global SST can reproduce the long term rainfall variability over northern Argentina which mainly shows an extended period of rainfall below the mean during 1930-1970 and rainfall above the mean since then. The correlation between observed and simulated evolutions over the 106 years is 0.34 and grows to 0.59 after a smoothing of 9 years to highlight interdecadal time scales, both values statistically significant at 5% level (see section 2.3). Therefore, since there is no inhomogeneity in the model output the similarity between model simulations and the GPCC data provides enhanced confidence in the observed long term variability, with the exception of the beginning of the 20th century. As shown below the CRU data set also shows the 1970 transition.

2.3 Methodology

The signal forced by the oceans is found performing a Maximum Covariance Analysis (MCA) between rainfall and the SST during JFM. The resulting modes are called SVDs because the MCA involves a singular value decomposition of the cross-covariance matrix, although here we used the correlation matrix between fields in the MCA in order to not take into account the different variances of rainfall and SST. In the case of model data we considered the ensemble mean precipitation from each experiment because the average procedure filters out a large portion of the noise variance allowing to separate the signal more clearly. The standard deviation was introduced back when plotting in order to represent anomaly fields with the right units. To relieve the aliasing problem the frequencies higher than 1/12 month^{-1} were filtered using a low-pass Lanczos filter to all year data before sampling the summer season (e.g. Zhou and Lau 2001).

The MCA is performed between the continental precipitation within 20°S-50°S and the SST field within [60°S-80°N, 0-360°E]. As mentioned in the introduction, precipitation variability in the region of interest is strongly associated with the ENSO phenomenon. Since we are focusing on interdecadal time scales we remove the interannual ENSO-related variability previous to the MCA in both precipitation and SST data sets. In order to do so, but keeping the long term variability in the tropical Pacific, we proceeded in the following way: 1) construct the Nino3.4 index in January-March (JFM), 2) use the Pacific Decadal Oscilation index in JFM to remove PDO-related variability from Nino3.4 through a linear regression procedure, and 3) remove the interannual Nino3.4-related variability from SST and precipitation data through a linear regression. The PDO time series was downloaded from http://jisao.washington.edu/pdo/PDO.latest. In the following we also use the AMO index (http://www.esrl.noaa.gov/psd/data/timeseries/AMO/) to determine the relationship between SVD modes and the AMO.

All data sets, simulated or observed, were linearly detrended previous to analysis; anomalies are always constructed based on the period 1901-2006. Statistical significance in the correlation analysis is calculated using the Student t-test. In the case of interannual variability (raw time series) we considered each year as independent, which results in (106-2) degrees of freedom. Correlations are tested at the 5% significance level.

After the MCA is performed, and in order to highlight the low-frequency behavior, the time series were band-passed with a 9-point running mean, resulting in time series that only include variability longer than a decade. In this case, to take into account the smoothing procedure, only 10 degrees of freedom were considered in the t-test, resulting that correlation values larger than 0.5 are significant at 5% level.

The statistical significance of anomalies between two chosen decades was assessed using the Monte Carlo method (Mo and Berbery 2011). In this method we compute the difference of the means of two decades constructed by taking randomly selected years from the same time series. The process is repeated 1000 times, allowing the statistical significance at each grid point to be calculated based on the empirical distribution function.

3. Observed interdecadal covariability between rainfall and SST

Figure 5 shows the first three observed SVD modes between observed (GPCC) rainfall in subtropical south America and global SST. The leading SVD (SVD1O) explains 28% of the covariance and the anomaly patterns suggest the remote influence of the PDO. The rainfall maximum is over southern Brazil-northern Uruguay and extends westward toward northern Argentina. The SVD1O time series of rainfall and SST are strongly correlated with the PDO index (see table I), such that a negative phase of the PDO induces negative rainfall anomalies, and show a clear change of sign in the mid-70s (from negative to positive anomalies), a characteristic of the PDO index (e.g. Mantua et al 1997). Furthermore, the correlation value between the evolution of rainfall time series and the PDO index increases to -0.7 on interdecadal time scales (table I).

The second SVD mode (SVD2O) explains 14% of the total covariance and the rainfall anomalies are dominated by an east-west dipole with centers over Uruguay and western northern

Argentina. The SST pattern shows negative anomalies over the tropical south Atlantic and positive anomalies south of 30°S and in the eastern Pacific. The SST SVD2O time series is not correlated with the PDO index, but is correlated with the AMO index at interannual and interdecadal time scales (table I). The rainfall time series is, however, not correlated to PDO or AMO.

The third SVD mode (SVD3O) explains approximately 11% of the covariance and represents the covariability between precipitation in southern Brazil, Paraguay and northeastern Argentina and most of the global oceans. In particular, the SST and rainfall time series of SVD3O are significantly correlated with both the PDO and AMO indices on interanual time scales (table I). On interdecadal time scales the SST time series is correlated with PDO and with the AMO indices, while the rainfall time series is significantly correlated only with AMO (table I).

The three observed SVDs suggest that rainfall anomalies in subtropical South America have large interdecadal fluctuations and are influenced by the PDO and AMO. In particular, the variability over northern Argentina seems to be mainly represented by the first two SVDs, the first showing a strong correlation with the PDO. The correlation of the SST time series of SVD2O with the AMO is puzzling because the north Atlantic, the main region of the AMO, only shows very weak SST anomalies (though significant). Instead, SVD2O shows larger significant anomalies in the equatorial-tropical south Atlantic. It is possible that the SVD2O mode is strongly influenced by internal atmospheric variability or by other processes that obscures the AMO signal. Moreover, from observations alone it is not possible to distinguish co-variability from causality. Thus, in order to further understand the impact of the oceans on rainfall variability we turn to model simulations.

4. Simulated interdecadal covariability between rainfall and SST

4.1 Impact of the global oceans

The first row of figure 6 shows the patterns and associated time series of the first SVD (SVD1G) from the GOGA-AL experiment. As for observations, it mainly shows the impact of the PDO over precipitation in subtropical South America, but explains more than double (about 63%) of the covariance between precipitation and SST. The simulated precipitation anomaly is located to the northwest of the observed anomaly, a known bias of the model for the Pacific influence in this region (see for example Barreiro and Diaz 2011). Nevertheless, it is clear that the model captures the signal adequately as the time series associated with the SST and rainfall anomalies are highly correlated with the PDO index (table II). The SVD1G is also correlated with the AMO index (table II), which is evidenced by a significant SST anomaly over the north Atlantic. On interdecadal time scales, however, the rainfall time series is only significantly correlated with the PDO (-0.72). The SVD1G time series associated with precipitation is also correlated with the corresponding rainfall series of the observed first three SVD modes, but only marginally with SVD2O and SVD3O (table II).

The second SVD (SVD2G, explains 12.5% of the covariance) reveals enhanced precipitation over northern Argentina accompanied by cold conditions in the equatorial-tropical south Atlantic and warm waters south of 20°S (second row of Figure 6). Moreover, most of the northern (southern) hemisphere extratropics tend to show negative (positive) SST anomalies. The rainfall and SST time series are characterized by interannual variability superimposed on a long term interdecadal swing that dominates the overall behavior. They are correlated at 0.6 which grows to 0.83 on interdecadal time scales, both statistically significant at 5% level. SST anomalies are relatively weak with peak-to-peak amplitudes of about 0.4 °C. Rainfall anomalies have a peak-to-peak amplitude of 0.6 mm/day, which should be compared with climatological means of about 3-4 mm/day (Figure 1). The rainfall time series of this SVD2G is significantly correlated with that of the second observed SVD (SVD2O), although the simulated rainfall pattern does not show anomalies over Uruguay (table II). Moreover, the rainfall time series is marginally correlated with the AMO (r=-0.51) on interdecadal time scales. Lastly, the SST patterns associated with the simulated and observed SVD2s show similar anomalies over the Atlantic.

As will be shown later, this mode of variability plays an important role in the behavior of rainfall over northern Argentina in the last decades, and thus it is analyzed in more detail. Figure 7 shows the regression of rainfall, 200mb geopotential height and vertically integrated moisture flux onto the time series of rainfall associated with SVD2G. As can be seen, enhanced rainfall over northern Argentina is accompanied by a weak Intertropical Convergence Zone (ITCZ) and stronger SACZ, particularly over the ocean. There is also a tendency for a southward shift of the Indo-Pacific ITCZ, although it is significant only over the Indian ocean and maritime continent (see section 4.3). At upper levels there is a clear dipole representing a strong Southern Annular Mode (SAM), characterized by stronger westerlies at 50-60°S and weakened westerlies at about 30-40°S, which induce reduced rainfall over southern Chile and the Patagonia. Note that a recent study shows that weaker westerlies are correlated with weaker (stronger) rainfall to the west (east) of the Andes (Garreaud et al 2013). The increased rainfall over Patagonia is not captured in our simulations probably because the low resolution of the model can not represent the steep topography of the region. The positive anomalies of geopotential height has superposed 4 maxima, one of which is close to southern South America, next to the Patagonian coast. This anticyclonic anomaly has a barotropic structure and influences the surface flow bringing more moisture from the Atlantic into northern Argentina. Convergence of this flow, together with increased evaporation (not shown), supports increased rainfall there.

These results suggest that the oceans can induce atmospheric anomalies that project onto SAM. Several studies have shown that SAM is primarily an internal mode of variability arising from eddy-mean flow interaction (e.g. Thompson and Wallace 2000, Limpasuvan and Hartmann 1999). However, it also has been shown that SAM can be influenced by external forcing from the tropical SST (e.g. Ding et al 2012). Seager et al 2003 report, for example, that ENSO projects strongly onto SAM. Recently, Yu and Lin (2013) show that the tropical Atlantic forcing dominates over forcings in the tropical Pacific or Indian ocean for the SAM trend and interannual summertime variability.

The third SVD (SVD3G) explains 7% of the covariance and anomalies reveal a weak rainfall dipole over subtropical South America covarying with negative SST anomalies in the tropical south Atlantic and warm anomalies in the eastern Pacific. There are also significant SST anomalies over the north Pacific. The time series of precipitation of SVD3G is marginally correlated with that of SVD2O (table II).

The analysis of the model simulations further supports that subtropical rainfall in South America shows large interdecadal variability and is influenced by PDO and AMO. Moreover, a cold tropical south Atlantic is apparently able to force significant atmospheric anomalies in the southern hemisphere that influence rainfall over northern Argentina. To further clarify the influence of the different ocean basins we turn to experiments POGA-AL and NAOGA-AL.

4.2 Impact of the Pacific ocean

The covariability between precipitation and SST in experiment POGA-AL is strongly dominated by the first SVD (SVD1P) that explains 72% of the covariance (Figure 8). As expected it shows the influence of the PDO on subtropical rainfall with patterns of SST and rainfall that are very similar to the first SVD of GOGA-AL. The rainfall time series of SVD1P is correlated with that of SVD1O at 0.37, with that of SVD3O at -0.23 and with the PDO index at -0.71. Thus, this experiment confirms the dominant role of the PDO on interdecadal rainfall variability over the subtropics, including northern Argentina. Regression of southern hemisphere precipitation onto the time series of rainfall associated with SVD1P shows a weakening of the Indo-Pacific ITCZ, an enhancement of the Atlantic ITCZ and in northern South America as well as negative rainfall anomalies in subtropical South America (Figure 9). Regression also shows anomalous northward flux from the subtropics to the Amazon basin flanked by a cyclonic circulation in eastern Brazil and an anticyclonic circulation centered at about 40°S over Argentina. This configuration reduces the southward climatological transport of moisture consistent with the simulated decreased subtropical rainfall. On upper levels there are positive geopotential height anomalies in a belt centered at 40°S with 4 centers, one of them located in South America.

The second and third SVDs show mainly interannual variability and are not considered here.

4.3 Impact of the tropical-North Atlantic ocean

The leading SVD (SVD1N, 45% of covariability) of experiment NAOGA-AL represents the impact of the north Atlantic basin on rainfall over subtropical south America. The SST pattern strongly resembles that of the AMO and the time evolution is correlated at r=-0.49 with the AMO index and grows to -0.86 on interdecadal timescales (Figure 10). The rainfall time series is correlated with the corresponding one of SVD3O (r=-0.2). The pattern, however, shows very weak anomalies that, even though they are significant, they are smaller than 0.1 mm/day over northern Argentina, which might be the reason why the observed SVD3O does not show significant rainfall anomalies over this region. Over the Southern hemisphere, regression onto the rainfall time series of SVD1N shows a southward shifted ITCZ over South America as expected for a cold tropical north Atlantic (Figure 11). Moreover, the ITCZ also shifts over the Indian ocean and western Pacific. Upper levels show an enhanced SAM, similar to that shown for SVD2G. However, in this case the anticyclonic circulation in the Atlantic sector is located over the continent, instead of to the east of the Patagonian coast (compare Figures 7 and 11) such that now the moisture flow is weaker and converges only weakly over northern Argentina.

The second SVD (SVD2N) explains 25% of the covariability and shows increased precipitation over northern Argentina associated with a cross-equatorial SST gradient in the tropical Atlantic with negative anomalies on the equator and to the south. The rainfall time series of SVD2N is significantly correlated with that of SVD2G (r=0.37) and with that of SVD2O (r=0.34), but is not correlated with the AMO index. The regression of southern hemisphere precipitation onto the time series of rainfall associated to SVD2N shows a weak and southward shifted ITCZ, an enhanced oceanic SACZ and decreased rainfall in southern Chile (Figure 12), as in the regression using the time series of SVD2G (Figure 7). Moreover, the southward shift of the ITCZ in the Indian ocean is also recovered, suggesting a remote forcing of the tropical Atlantic as in the case of SVD1N, although with weaker amplitudes. The mechanism of this connection is not a concern of this study, but it might be related to that found by Kucharski et al (2009) in a different season. In upper levels the regression shows anomalies characteristic of a stronger SAM and a clear anticyclone next to the Patagonian coast with about 75% of the intensity found in the regression of SVD2G. In the tropics there is overall decrease of geopotential height as expected due to a colder tropical Atlantic. The pattern of cyclonic and anticyclonic geopotential height anomalies at about 20°S and 45°S, respectively, over South America is very similar to the Rossby wave train found by Seager et al (2010) when forcing another AGCM with a cold tropical Atlantic during austral winter. Regression of the integrated moisture flux also recovers a pattern similar to that of SVD2G. Comparison of Figures 7 and 12 then demonstrates that the increased rainfall over northern Argentina, and most of the anomalies associated with SVD2G, are the result of a cold equatorial-tropical south Atlantic, and are not related to AMO. Anomalies are generally weaker, except in the tropical Atlantic, but the spatial structure is very similar.

The third SVD mode of NAOGA-AL is dominated by interannual variability and is not considered here.

The analysis of the SVDs of NAOGA-AL together with those of GOGA-AL and GPCC suggests that the AMO has a significant but weak influence on rainfall variability over northern Argentina and that its impact might be seen as a long time scale modulation of the impact from the tropical Pacific basin (as proposed recently by Mo and Berbery 2011) instead of in isolation. At the same time, the cross-equatorial SST gradient with largest weight in the south Atlantic (independent of AMO) that characterizes the second SVD modes of GPCC, GOGA-AL and NAOGA-AL can have a stronger impact than AMO on rainfall over northern Argentina during southern hemisphere summer. Together, these results suggest that the second SVD mode of GOGA-AL (SVD2G) has components of both AMO and the cross-equatorial SST gradient leading to a larger rainfall anomaly over northern Argentina.

It is worth mentioning that atmospheric internal variability associated with an intensification of the south Atlantic anticyclone induces cold (warm) SST anomalies north (south) of 20°S, inducing an SST pattern at the end of the austral summer similar as that represented in SVD2G (Barreiro et al 2004). Here we showed that the northern lobe is the one playing the major role in forcing rainfall anomalies, as expected from our current understanding of the impact of the tropical versus extratropical SST anomalies on atmospheric circulation.

5. Long term behavior of precipitation over northern Argentina

Figure 13 shows the long term behavior of the observed (GPCC) rainfall over northern Argentina together with the time series of precipitation associated with the first two SVD modes of GOGA-AL (SVD1G and SVD2G). It is easily seen that SVD2G follows more closely the long term behavior of the observed precipitation. In fact, after neglecting the first decade in which the two time series are out of phase, from 1910 onwards the correlation between SVD2G and precipitation in northern Argentina is 0.7, significant at 5% level. (The opposite behavior seen in the first decade of the century might be a result of the limited number of observations during that time (Figures 2, 3).) On the other hand, the correlation between SVD1G and precipitation in northern Argentina on interdecadal time scales is not statistically significant. Moreover, SVD2G captures very well the evolution of the observed precipitation over northern Argentina during the transition from a dry period in 1950-1960 to a wet period that started in the 1970s, the largest transition on record. Interestingly, the time series of the SVD1G, that characterizes the PDO influence, suggests that while the PDO did not play a role in the transition, it did play a role in maintaining the wet conditions from 1980 to the end of the record.

To diagnose the atmospheric anomalies that accompany the long term precipitation variability in northern Argentina we computed the difference between the decades before and after the 1970s transition: we considered the periods (1959-1968) and (1975-1984), respectively (see Figure 13). These periods are within the time span of largest coverage of rain gauges in the area of interest (see Figure 2) and there are reanalysis data sets available to compare with model simulations. According to the time series, anomalies will have components of SVD1G and SVD2G. Notice that in the model rainfall anomalies during (1959-1968) evolve from positive to negative, while they are consistently positive during (1975-1984) as in observations.

Figure 14 shows a comparison between the precipitation in the decades before and after the transition for the ensemble mean of experiment GOGA-AL and GPCC over South America. It can be clearly seen that the map of GOGA-AL is quite similar to that of the GPCC data set: they both show increased rainfall over northern Argentina and between [10°S-20°S, 70°W-65°W] to the east of the Bolivian Altiplano as well as a weaker ITCZ. On the other hand, the simulated rainfall increase in northern Argentina does not extend as far south as in observations and also shows enhanced rainfall in eastern Brazil between 10°S-20°S that is only suggested in GPCC. The CRU data set (Figure 15a) shows similar features, including enhanced rainfall in eastern Brazil between 10°S-20°S.

On the other hand, the precipitation anomalies in the three reanalyses (NCEP-CDAS1, ERA40 and 20th Century) show significant different features. First of all, they present strong positive rainfall anomalies over the whole Amazon region that are not present in observations (Figures 15b,c,d). Also, ERA40 shows a weakened SACZ, while the 20th century and NCEP CDAS-1 reanalyses show an enhanced SACZ. The 20th century reanalysis appears to be the closest to observations because there is a hint of decreased rainfall in northeast Brazil and shows increased rainfall in northern Argentina, although only in the southern part. NCEP-CDAS1 shows maximum rainfall over Uruguay where observations show no significant anomalies and ERA40 does not show a consistent signal over northern Argentina.

Furthermore, the difference of 200 mb geopotential height between decades across the transition for NCEP CDAS1 and the 20th Century reanalyses show large differences (Figure 16). While in the northern hemisphere extratropics the patterns of anomalies in the reanalyses coincide (although with different amplitude), in the southern hemisphere anomalies are of opposite sign over large regions. Particularly, over southern South America the 20th Century reanalysis shows a cyclonic circulation centered off the Patagonian coast, while the NCEP CDAS1 shows positive height anomalies south of 20°S. To allow comparison the figure shows anomalies with respect to the period 1949-2006 for both data sets, but in the case of the 20th century reanalysis the results do not change significantly if the period 1901-2006 is considered. The differences in the southern hemisphere in different reanalyses is not surprising given the lack of observations in the southern extratropics previous to the satellite era, that is, before 1979 (Sterl 2004).

The substantial differences between reanalysis products and observed rainfall anomalies, together with different upper level atmospheric circulation anomalies in different reanalyses precludes us from using them to study the atmospheric circulation anomalies associated with the observed rainfall differences, and at the same time validate the model. On the other hand, given that the model does a reasonable job in representing the observed rainfall anomalies over whole South America (Figure 14) we expect that the atmospheric circulation processes associated with the climate transition in the 1970s are well represented.

The SST field accompanying the transition in the 1970s reveals warm conditions in the eastern Pacific and south Atlantic oceans as well as a cold equatorial Atlantic (Figure 17a). The output of GOGA-AL shows that in upper levels the extratropical atmosphere is dominated by a barotropic anticyclonic anomaly that weakens westerly winds at 30°S, increases northerly winds in the South American subtropics and westerlies south of 40°S (Figure 17b). The location of the upper level anticyclone is very similar to that seen in SVD2G (Figure 7).

On seasonal time scales precipitation is balanced by the convergence of moisture advected into the region by the winds and local evaporation. Thus, Figure 17c,d show the moisture flux integrated from top to bottom of the atmosphere as well as its divergence and the evaporation anomalies. Because of data availability from the simulations the moisture transport was calculated using the monthly mean fields of winds and specific humidity, and thus it does not consider the contribution of the synoptic eddies. The plots show that the positive precipitation anomalies seen in Figure 14b are the result of both enhanced local evaporation and moisture convergence by the mean flow. On the other hand, the weakened ITCZ region is mainly result of anomalous moisture divergence, except in northern South America where decreased moisture is also important. Over northern South America there is increased moisture transport from the equatorial Atlantic into the Amazon region, probably as consequence of the SST gradient resulting from a cold Atlantic and warm equatorial Pacific (e.g. Barreiro and Tippmann 2008). The moisture flux turns southward due to the Andes topographic barrier joining the increased moisture flux coming from the south Atlantic due to the extratropical anticyclonic anomaly. As a result there is convergence of moisture over northern Argentina, which together with increased evaporation leads to increased precipitation in the region. Consistently, the anomalous vertical velocity at 500 mb shows enhanced ascent over northern Argentina (not shown). There is also a noticeable contribution of the eddy field to the moisture convergence over northern Argentina that can be estimated as the difference between the precipitation and the sum of evaporation and moisture convergence of the mean flow.

6. Effect of land-atmosphere interaction

In this section we are interested in addressing the role of the interaction between moisture anomalies and the atmospheric circulation in the rainfall response to remote forcing. The results of the previous section were found allowing the soil moisture to change due to rainfall variability and then feed back to the atmosphere in the form of enhanced or reduced evaporation. Here we consider the output of an experiment where soil moisture is prescribed to a climatological value (GOGA). As before the model is forced with global SST and a 9-member ensemble is constructed.

The lack of land-atmosphere interaction modifies the evolution of summertime precipitation in northern Argentina. In the absence of soil moisture feedback the model captures some of the observed variability as the correlation of simulated rainfall anomalies with observations over northern Argentina is 0.25 during the 106 years (Figure 18). This value is statistically significant but appreciably smaller than when soil-moisture varies with precipitation (0.34). Moreover, the differences are larger when considering the long term evolution: while with soil-moisture feedback the correlation is 0.59 (statistically significant at 5% level), in its absence the correlation drops to 0.26 which is not significant. The lack of correlation on long time scales is clearly seen in figure 18, where the two time series are out of phase during the first 60 years of the century, and only tend to behave similarly in the last 40 years.

To further address the role of soil moisture feedback we plot the precipitation difference between periods (1975-1984) and (1959-1968) for individual ensemble members (Figure 19). Clearly, the dispersion of rainfall anomalies is larger for GOGA than for GOGA-AL ensemble members. In fact, while all ensemble members show positive anomalies in the case of GOGA-AL, there are two ensemble members of GOGA that show negative values, the opposite from observations. On the other hand, some GOGA members reach higher values, closer to the one seen in the GPCC and CRU data. Thus, interactive soil moisture allows a more consistent response among ensemble members, increasing the signal-to-noise ratio and results in a better representation of the impact of the oceans on precipitation over northern Argentina.

7. Summary and discussion

The study explored the SST-forced signal in summertime precipitation over subtropical South America using observations and tailored experiments that separate the contributions of the Pacific and tropical-north Atlantic SST anomalies on long time scales. Moreover, the role of land-atmosphere interaction was assessed analyzing the results of twin experiments with and without soil moisture feedback. We focus on northern Argentina because it is the region with more uniform rain gauge coverage over the whole 20 century in the observed (GPCC) data set, thus providing best confidence in the results. In this region it is also located Laguna Mar Chiquita, a lake that has shwon large interdecadal variability over the last 200 years (Piovano et al 2004). The results of this study provides important information about the oceanic forcing that has dominated this region in the last century and may have affected the evolution of the lake level.

After removing the interannual ENSO signal, a MCA between the observed precipitation and SST fields during January-March reveals three first modes that together explain more than 50% of the covariability. These modes show substantial interdecadal variability and suggest the impact of the Pacific Decadal Oscillation, the Atlantic Multidecadal Oscillation and the tropical Atlantic SST on rainfall variability in subtropical South America. The first mode is associated with the PDO and suggests that its influence is largest over southeastern South America extending over northern Argentina, and is such that a negative PDO induces negative rainfall anomalies. These results are in agreement with previous studies (e.g. Kayano and Andreoli 2007). The second mode associates a rainfall dipole over subtropical South America mainly with a cold equatorial-tropical South Atlantic and warm eastern Pacific. Finally, in the third observed mode negative rainfall anomalies in south Brazil and Paraguay are correlated with positive PDO and AMO. The difficulty in interpreting the role of individual basins motivated us to analyze model simulations where the AGCM is forced imposing different SST fields as boundary conditions.

When forced with global historical SST the model captures the impact of the PDO on subtropical rainfall (as the leading mode with 63% of covariability), although a bias of the model puts the maximum anomalies to the northwest of the observed pattern. This influence is further verified in an experiment where the AGCM is forced with Pacific-only SST anomalies.

The second SVD mode of the model forced with global SST anomalies shows enhanced precipitation over northern Argentina accompanied by cold (warm) sea surface conditions north (south) of 20°S in the Atlantic basin. A south-north equatorial SST gradient is also apparent in the Atlantic. The rainfall time series is correlated with that of the second observed SVD, and with the AMO on interdecadal time scales. Even though the SST patterns in the Atlantic are similar in observations and model simulations (SVD2O and SVD2G), rainfall anomalies in the model are concentrated over northern Argentina, while in observations the rainfall pattern is characterized by a dipole structure with opposite anomalies in Uruguay and northern Argentina. These differences may reflect the existence of large internal atmospheric variability in observations, or model biases.

To further explore the impact of the Atlantic ocean on northern Argentina's rainfall we analyzed the output of an experiment where the AGCM is forced with SST anomalies restricted to that basin north of 20°S. The MCA revealed a first mode dominated by the AMO with weak influence on rainfall over subtropical South America, and a second SVD mode characterized by the impact of a cross-equatorial SST gradient such that a south-north gradient induces increased rainfall over northern Argentina. Comparing these modes with the second mode of the experiment forced with global historical SST (SVD2G), suggests that the rainfall anomalies in the latter are mainly forced by the cross-equatorial SST gradient dominated by the equatorial-tropical south Atlantic. Moreover, according to this experiment, both the AMO and the tropical south Atlantic force a barotropic anticyclonic circulation in the southwestern Atlantic that is crucial for changing summertime rainfall in northern Argentina. Seager et al (2010) showed that a cold tropical Atlantic also forces a similar anticyclone during winter. The position and strength of the forced anticyclone is not very different in the case of a cold AMO and a cold equatorial-tropical south Atlantic, but the moisture convergence and rainfall anomalies over northern Argentina are significantly different. Thus, relatively small changes in the characteristics of the anticyclone leads to significant differences in climate anomalies over northern Argentina, and future work should address the particular physical processes that lead to the establishment of this circulation anomaly during summertime as well as its sensitivity to SST and model formulation.

The long term behavior of rainfall over northern Argentina is characterized by a strong change at the beginning of the 1970s, from decades of unusually dry conditions to decades of unusually wet conditions. We found that the rainfall time series associated with the second SVD of the AGCM forced with global SST (SVD2G) captures very well this transition, which suggests that the Atlantic basin is the main responsible for this transition. We further found that the mode associated with the PDO changed phase in late 1970s and helped maintain wet conditions after 1980. The observed rainfall difference across the transition over South America shows enhanced rainfall not only in northern Argentina, but also within [60-70°W,10-20°S] and to the north of 5°N. On the other hand, it shows a weakened ITCZ. The model simulation is able to reproduce these changes, particularly those over northern Argentina, and except over Venezuela where they present anomalies of the opposite sign. Data from reanalyses, on the other hand, are not able to reproduce the observed rainfall changes over northern Argentina and show strong anomalies in the Amazon basin that are not present in observations. Moreover, reanalysis products show very different anomalies in upper levels in the southern hemisphere across the transition. These deficiencies did not allow to use the reanalysis data sets to validate the model.

According to model simulations, the 1970s rainfall transition is characterized by a cold equatorial Atlantic and a warm equatorial Pacific which induce enhanced moisture transport into the Amazon region part of which turns south when it encounters the Andes. Moreover, upper levels are dominated by a strong extratropical anticyclone located at about (40°W,40°S) that due to its barotropic vertical structure is able to influence the surface flow. These two processes increase the moisture transport and convergence in northern Argentina leading to enhanced rainfall there.

These results tend to agree with those of Seager et al (2010) on the importance of the Atlantic for interdecadal variability in subtropical South America, even tough we focus on a different season. Recently, Mo and Berbery (2011) found that a warm equatorial Pacific and a cold tropical north Atlantic is the best combination for increasing the persistence of wet spells in subtropical South America, including the area of interest of this study (northern Argentina). Our results suggest that the impact of the Atlantic ocean on rainfall in northern Argentina is mainly associated with a cold equatorial-tropical south Atlantic that induces positive anomalies (SVD2G, SVD2N). On the other hand, assuming linearity in the response, a cold tropical north Atlantic (SVD1N) and a warm tropical Pacific (SVD1P) will also tend to interact constructively to induce stronger rainfall over that area, but not in other subtropical regions.

Finally, we found that land-atmosphere interaction leads to a rainfall evolution over northern Argentina that is closer to the observed one during the whole 20th century. Moreover, allowing soil moisture feedback leads to a signal that has smaller dispersion among ensemble members, and thus larger signal-to-noise ratio. In the absence of interactive soil moisture the simulated rainfall anomaly shows large variability among ensemble members such that when considering the difference between two decades the anomaly over northern Argentina can be of the opposite sign compared to observations.

Our results, together with those of previous authors, reinforce the idea that rainfall over subtropical South America may have some predictability on interdecadal time scales provided the sea surface temperature anomalies are known in advance. This opens an interesting possibility and asks for more research on a topic that has very important societal applications. Future studies should include the representation of this variability in coupled climate models and its interaction with the anthropogenic signal.

Acknowledgements

The research leading to these results has received funding from the European Community's Seventh Framework Programme (FP7/2007-2013) under Grant Agreement N° 212492 (CLARIS LPB a Europe-South America Network for Climate Change Assessment and Impact Studies in La Plata Basin) and from CSIC-Universidad de la República. We are also grateful to three reviewers for their valuable suggestions that greatly improved the manuscript.

References

Andreoli RV, Kayano MT (2005) ENSO related rainfall anomalies in South America and associated circulation features during warm and cold Pacific Decadal Oscillation regimes. Int. J. Climatol., 25, 2017-2030.

Antico PL (2008) Relationships between autumn precipitation anomalies in southeastern South America and El Niño events classification. Int. J Climatology 29: 719-727, doi: 10.1002/joc.1734.

Barreiro M, Diaz N (2011) Land-atmosphere coupling in El Niño influence over South America. Atmos Sci Lett 12:351-355, doi: 10.1002/asl.348.

Barreiro M (2010) Influence of ENSO and the south Atlantic ocean on climate predictability over Southeastern South America. Clim Dyn 35:1493-1508, doi: 10.1007/s00382-009-0666-9.

Barreiro M, Tippmann A (2008) Atlantic modulation of El Niño influence on summertime rainfall over Southeastern South America. *Geophys Res Lett 35, doi:10.1029/2008GL035019.*

Barreiro M, Giannini A, Chang P, Saravanan R (2004) On the role of the South Atlantic atmospheric circulation in Tropical Atlantic Variability. *In Earth's Climate: The Ocean-*Atmosphere Interaction, Eds. Wang, Xie and Carton, Geophysical Monograph Series 147, AGU, Washington DC, pp 143-156.

Baldi G, Paruelo JM (2008) Land-use and land cover dynamics in South American temperate grasslands. Ecol Soc 13(2), 6.

Boulanger J-P, Leloup J, Penalba O, Rusticucci M, Lafon F, Vargas W (2005) Observed precipitation in the Paraná-Plata hydrological basin: long-term trends, extreme conditions and ENSO teleconnections. Clim Dyn 24: 393-413. doi: 10,1007/s00382-004-0514-x

Cazes-Boezio G, Robertson AW, Mechoso CR (2003) Seasonal dependence of ENSO teleconnections over South America and relationships with precipitation in Uruguay. J. Climate, 16:1159–1176.

Castañeda E, Barros V (2001) Tendencias de la precipitación en el oeste de Argentina.

Meteorologica 26: 5-23.

Chan SC, Behera SK, Yamagata T (2008) Indian ocean dipole influence on South American rainfall. Geophys. Res. Lett. doi:10.1029/2008GL034204 .

Collini EA, Berbery EH, Barros VR, Pyle ME (2008) How does soil moisture influence the early stages of the South American monsoon? J. Climate 21: 195–213.

Compo, GP., Whitaker JS, Sardeshmukh PD, Matsui N, Allan RJ, Yin X, Gleason BE, Vose RS, Rutledge G, Bessemoulin P, Brönnimann S, Brunet M, Crouthamel RI, Grant AN, Groisman PY, Jones PD, Kruk M, Kruger AC, Marshall GJ, Maugeri M, Mok HY, Nordli O, Ross TF, Trigo RM, Wang XL, Woodruff SD, Worley SJ (2011) The Twentieth Century Reanalysis Project. Quarterly J. Roy. Meteorol. Soc., 137: 1-28.

Ding Q, Steig EJ, Battisti DS, Wallace JM (2012) Influence of the tropics on the southern annular mode. J Clim 25: 6330-6348.

Fuchs T, Schneider U, (2009) GPCC Annual Report for year 2008. http://gpcc.dwd.de/

Garreaud R, Lopez P, Minvielle M, Rojas M (2013) Large scale control on the Patagonia climate. J Clim 26: 215-230.

Grimm AM, Ambrizzi T (2009) Teleconnections into South America from the tropics and extratropics on interannual and intraseasonal time scales, in Past Climate Variability in South America and sorrounding regions: from the Last Glacial Maximum to the Holocene, Developments in Paleoenvironmental Research and Risk Assessment, edited by F. Vimeux et al., pp. 159-191 doi:10.1007/978-90-481-2672-9.

Grimm AM, Pal J, Giorgi F (2007) Connection between spring conditions and peak summer monsoon rainfall in South America: role of moisture, surface temperature, and topography in eastern Brazil. J. Climate 20: 5929-5945.

Grimm AM, Barros VR, Doyle M (2000) Climate variability in southern South America associated with El Niño and La Niña events. J. Climate 13:35-58.

Grimm AM, Pal JS, Giorgi F (2007) Connection between Spring Conditions and Peak Summer Monsoon Rainfall in South America: Role of Soil Moisture, Surface Temperature, and Topography in Eastern Brazil. J. Climate 20:5929–5945. doi: http://dx.doi.org/10.1175/2007JCLI1684.1

Gonzalez P, Polvani LM, Seager R, Correa GP (2013) Stratospheric ozone depletion: a key driver of recent precipitation trends in South Eastern South America. Clim Dynam, DOI 10.1007/s00382-013-1777-x.

Harris I, Jones PD, Osborn TJ, Lister DH (2012) Updated high-resolution grids of monthly climatic observations - the CRU TS3.10 dataset. Submitted to International Journal of Climatology.

Kalnay E, Kanamitsu M, Kistler R, Collins W, Deaven D, Gandin L, Iredell M, Saha S, White G, Woollen J, Zhu Y, Leetmaa A, Reynolds B, Chelliah M, Ebisuzaki W, Higgins W, Janowiak J, Mo KC, Ropelewski C, Wang J, Jenne R, Joseph D (1996) The NCEP/NCAR 40-Year Reanalysis Project. Bull. A. Meteorol. Soc. 77:437-471.

Kayano MT, Andreoli RV (2007) Relation of South American summer rainfall interannual variations with the Pacific Decadal Oscillation. Int. J. Climatol 27:531-540.

Koster RD, Suarez MJ, Heiser M (2000) Variance and predictability of precipitation at seasonal-to-interannual timescales. Journal of Hydrometeorology 1: 26-46.

Koster RD et al. 2004. Regions of Strong Coupling Between Soil Moisture and Precipitation.

Science 305: 1138-1140.

Kucharski F, Molteni F, Bracco A (2005) Decadal interactions between the western tropical Pacific and the North Atlantic Oscillation. Clim Dyn, doi:10.1007/s00382-005-0085-5.

Kucharski F, Bracco A, Yoo JH, Tompkins AM, Feudale L, Ruti P, Dell'Aquila A (2009) A Gill-Matsuno type mechanism explains the tropical Atlantic influence on African and Indian monsoon rainfall. Q. J. R. Meteorol. Soc., DOI: 10.1002/qj.406.

Limpasuvan V, Hartmann DL (1999) Eddies and the annular modes of climate variability. Geophys Res Lett 26:3133-3136

Ma H-Y, Mechoso CR, Xue Y, Xiao H, Wu C-M, Li J-L, De Sales F (2010) Impact of land surface processes on the South American season climate. Climate Dynamics DOI:10.1007/s00382-010-0813-3.

Magrin GO, Travasso MI, Rodriguez GR (2005) Changes in climate and crop production during the 20th century in Argentina. Climatic Change 72:229–249.

Mantua NJ, Hare SR, Zhang Y, Wallace JM, Francis RC (1997) A Pacific interdecadal climate oscillation with impacts on salmon production. Bulletin of the American Meteorological Society 78 (6): 1069–1079.

Misra V (2008) Coupled air, sea and land interactions of the south American Monsoon. Journal of Climate 21: 6389-6403.

Mo KC, Berbery EH (2011) Drought and Persistent Wet Spells over South America based on Observations and the U. S. CLIVAR Drought experiments. J Climate 24:1801–1820.

Piovano E, Ariztegui D, Bernasconi S, McKenzie J (2004) Stable isotopic record of hydrological changes in subtropical Laguna Mar Chiquita (Argentina) over the last 230 years. The Holocene

14: 525-535.

Pisciottano G, Díaz A, Cazes G, Mechoso CR (1994) El Niño – Southern Oscillation impact on rainfall in Uruguay. J. Climate 7:1286-1302.

Renom M, Rusticucci M, Barreiro M (2011) Multidecadal changes in the relationship between extreme temperature events in Uruguay and the general atmospheric circulation. Clim Dyn 37:2471-2480, doi: 10.1007/s00382-010-0986-9.

Schneider U, Fuchs T, Meyer-Christoffer A, Rudolf B (2008) Global precipitation analysis products of the GPCC. Global Precipitation Climatology Centre Tech. Rep., 12 pp.

Seager R Harnick N, Kushnir Y, Robinson W, Miller J (2003) Mechanisms of hemispherically symmetric climate variability. J Clim 13:1000-1016.

Seager R, Naik N, Baethgen W, Robertson A, Kushnir Y, Nakamura J, Jurburg S (2010) Tropical oceanic causes of interannual to multidecadal precipitation variability in southeast South America over the past century. J Clim 23:5517-5539.

Silvestri G (2004) El Niño signal variability in the precipitation over southeastern South America during austral summer. Geophys. Res. Lett. doi:10.1029/2004GL020590.

Smith TM, Reynolds RW (2004) Improved extended reconstruction of SST (1854-1997). J Climate 17: 2466-2477.

Sorensson AA, Menéndez CG (2010) Summer soil-precipitation coupling in South America. Tellus Series A 63: 56-68.

Sterl, A (2004) On the in-Homogeneity of reanalysis products. J Clim 17:3866–3873.

Taschetto AS, Ambrizzi T (2012) Can Indian ocean SST anomalies influence South American rainfall? Clim. Dyn 38:1615–1628 .

Thompson DWJ, Wallace JM (2000) Annular modes in the extratropical circulation. Part I: Month-to-month variability. J Clim 13: 1000-1016.

Troin M, Vallet-Coulomb C, Sylvestre F, Piovano E (2010) Hydrological modeling of a closed lake (Laguna Mar Chiquita, Argentina) in the context of 20th century climatic changes. J Hydrology 393, doi: 10.1016/j.jhydrol.2010.08.019.

Uppala SM and coauthors (2005) The ERA-40 Reanalisys, Quart. J. Roy. Meteorol. Soc. 131, 612: 2961-3012.

Xue Y, De Sales F, Li W, Mechoso CR, Nobre C, Juang H-MH (2006) Role of land surface processes in South American monsoon development. Journal of Climate 19: 741–762.

Yu B, Lin H (2013) Tropical American-Atlantic forcing of austral summertime variability in the southern annular mode. Geophys Res Lett 40: 943-947, doi:10.1002/GRL.50231.

Zeng N, Neelin JD, Chou C. 2000. A quasi-equilibrium tropical circulation model – implementation and simulation. J Atmos Sci 57:1767-1796.

Zhou J, Lau K-M (2001) Principal modes of interannual and decadal variability of summer rainfall over South America. Int. J. Climatol. 21:1623-1644.

Tables

	SVD1O-S	SVD2O-S	SVD3O-S	SVD1O-P	SVD2O-P	SVD3O-P
PDO	-0.8 (-0.86)	*	0.59 (0.56)	-0.47 (-0.7)	*	0.25 (*)
AMO	*	-0.33 (-0.55)	0.57 (0.63)	*	*	0.28 (0.56)

Table I – Interannual correlation coefficients between the time series associated with the first three observed modes and PDO and AMO indices. SVD1O-S denotes the time series of SST associated with the first SVD mode; SVD1O-P denotes the time series of rainfall associated with the first SVD mode. Other SVD indices are analogous. Values within brackets indicate correlations on interdecadal time scales (after a 9-year smoothing). Only statistically significant correlation values at 5% level are shown.

	SVD1O-P	SVD2O-P	SVD3O-P	PDO	AMO
SVD1G-P	0.33	-0.2	-0.23	-0.61	-0.27
SVD2G-P	*	0.25	*	*	*
SVD3G-P	*	0.2	*	*	*

Table II - Interannual correlation coefficients between the time series of precipitation associated with the first three simulated modes and those of observed modes as well as AMO and PDO indices. SVD1G-P denotes the rainfall time series associated with the first SVD of the experiment where the AGCM is forced with global historical SST; other SVD indices are analogous. Only statistically significant values at 5% level are shown.

Figure captions

Figure 1 – January-March rainfall climatology (1901-2006) from GPCC data set (mm/day). The crosses indicate the area of northern Argentina.

Figure 2 – Total number of rain gauges in northern Argentina from 1901 to 2006 considered in the GPCC data set. Note the increase during the first half of the century and the decline after a peak in the 1970s.

Figure 3 – Average number of reporting gauges per grid cell in GPCC data set through the different decades of the XX century. The last contour of the scale is 30.

Figure 4 – Summertime evolution of rainfall averaged over northern Argentina in GPCC data (blue) and in ensemble mean of experiment where AGCM is forced with global SST (GOGA-AL, red). The thick curves represent the interdecadal variability computed as a 9-year running mean. Times series have been normalized.

Figure 5 – First three SVD modes between observed rainfall and SST. The first column shows the rainfall patterns, the second the SST pattern, and the third column the corresponding time series for precipitation (dashed) and SST (solid). SST and rainfall patterns in °C and mm/day, respectively. The shading indicates regions statistically significant at 5% level.

Figure 6 - First three SVD modes between rainfall and SST from ensemble mean of GOGA-AL. The first column shows the rainfall patterns, the second the SST pattern, and the third column the corresponding time series for precipitation (dashed) and SST (solid). SST and rainfall patterns in °C and mm/day, respectively. The shading indicates regions statistically significant at 5% level.

Figure 7 – Linear regression onto the rainfall time series of SVD2G of a) rainfall (mm/day), b)

200 mb geopotential height (m), c) vertically integrated moisture flux (g/cm/s). In a) the contours are (-1,-0.8,-0.6,-0.4,-0.2,-0.1,0.1,0.2,0.4,0.6,0.8,1) mm/day. Shaded areas are statistically significant at 5% level; in c) shading indicates that at least one component of the moisture flux is statistically significant.

Figure 8 – First SVD mode between rainfall and SST from ensemble mean of POGA-AL. Plots as in Figure 6.

Figure 9 – Analogous to Figure 7, but regression onto rainfall time series of SVD1P.

Figure 10 – First two SVD modes between rainfall and SST from ensemble mean of NAOGA-AL. Plots as in Figure 6.

Figure 11 – Analogous to Figure 7, but regression onto rainfall time series of SVD1N.

Figure 12 – Analogous to Figure 7, but regression onto rainfall time series of SVD2N.

Figure 13 – Long term evolution (9-yr smoothed) time series of observed rainfall in northern Argentina (blue), rainfall time series associated with the first (green) and second (red) SVD modes of GOGA-AL. Time series are normalized.

Figure 14 – Rainfall anomaly (contours, mm/day) between periods (1975-1984) and (1959-1968) over all South America for a) GPCC data, b) the ensemble mean of GOGA-AL. Shading indicates the regions statistically significant at the 10% level. The contour interval for GOGA-AL is 0.2 mm/day, while for the GPCC data set is 0.4 mm/day.

Figure 15 – Analogous to Figure 14, but for a) CRU, b) 20th century renalysis, c) ERA40 reanalysis, d) NCEP CDAS1 reanalysis.

Figure 16 – 200 mb geopotential height anomaly (contours, m) between periods (1975-1984) and (1959-1968) for a) 20th century reanalysis, b) NCEP CDAS1 reanalysis. Shading indicates

the regions statistically significant at the 10% level.

Figure 17 - Anomalies between periods (1975-1984) and (1959-1968) for different fields of experiment GOGA-AL. a) SST (°C), b) 200 mb geopotential height (m), c) vertically integrated moisture flux (g/cm/s) and its divergence (mm/day), d) evaporation (mm/day). Shading indicates the regions statistically significant at the 10% level.

Figure 18 – Analogous to Figure 4, but for GOGA experiment (AGCM with climatological soil moisture).

Figure 19 – Rainfall difference over northern Argentina between periods (1975-1984) and (1959-1968) in each ensemble member for GOGA experiment (blue) and GOGA-AL experiment (red) in mm/day. The green dots indicate the anomalies in GPCC data and the black asterisks in the CRU data. The horizontal axis is only drawn to separate data from GOGA-AL and GOGA experiments, it does not have units.

Figure 1

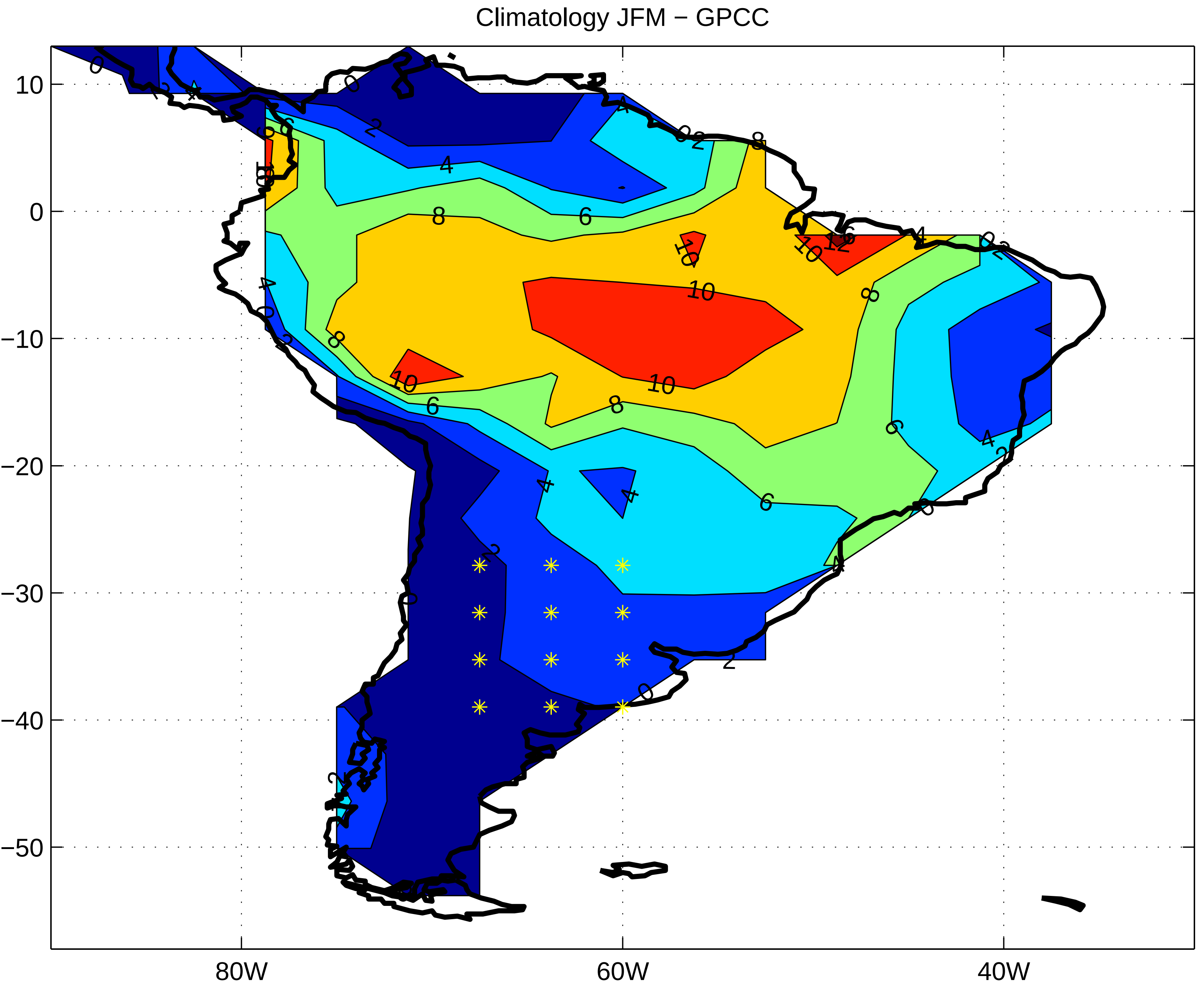

Figure 2

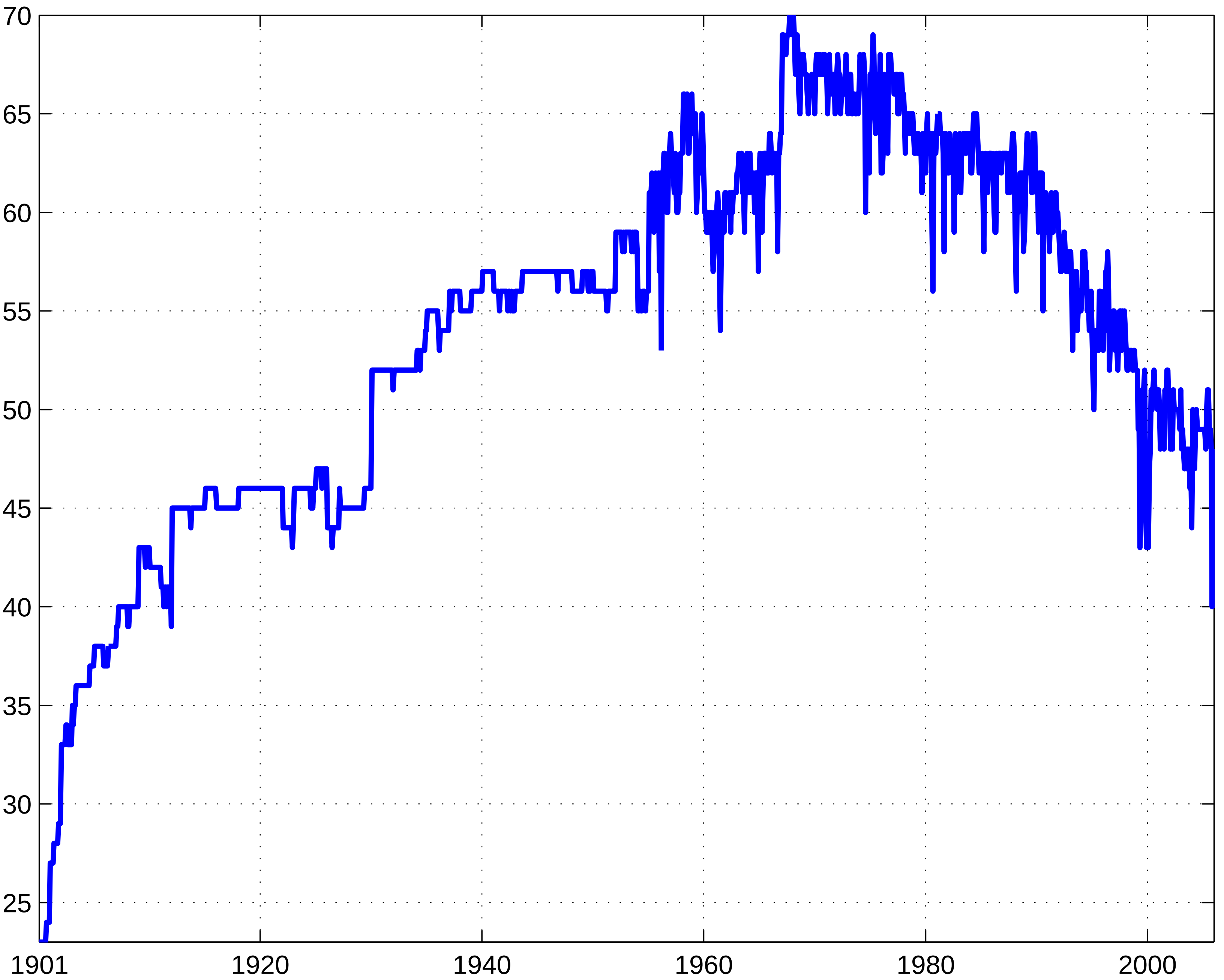

Figure 3

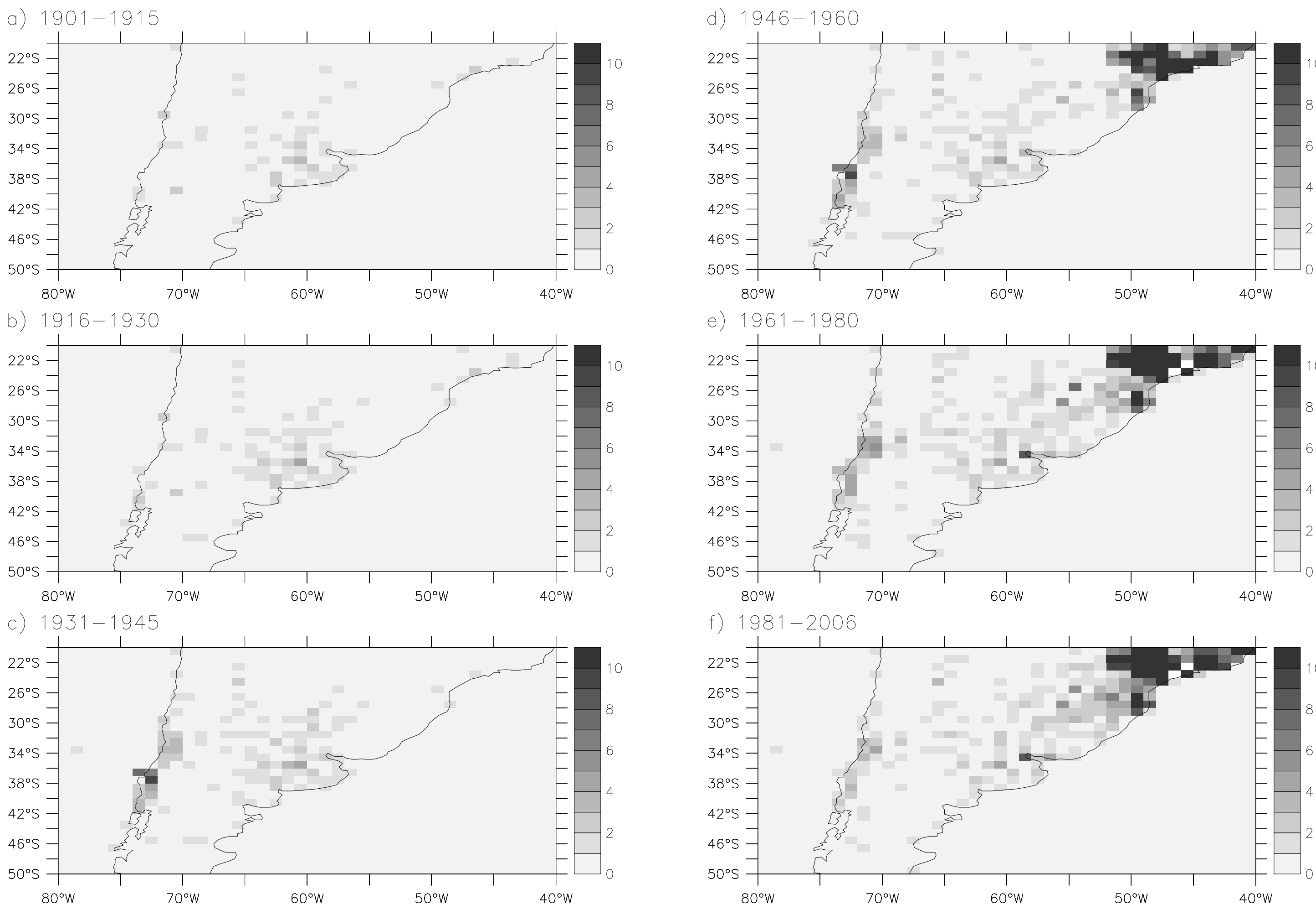

a) 1901–1915
b) 1916–1930
c) 1931–1945
d) 1946–1960
e) 1961–1980
f) 1981–2006
22°S
26°S
30°S
34°S
38°S
42°S
46°S
50°S
80°W
70°W
60°W
50°W
40°W
0
2
4
6
8
10

Figure 4

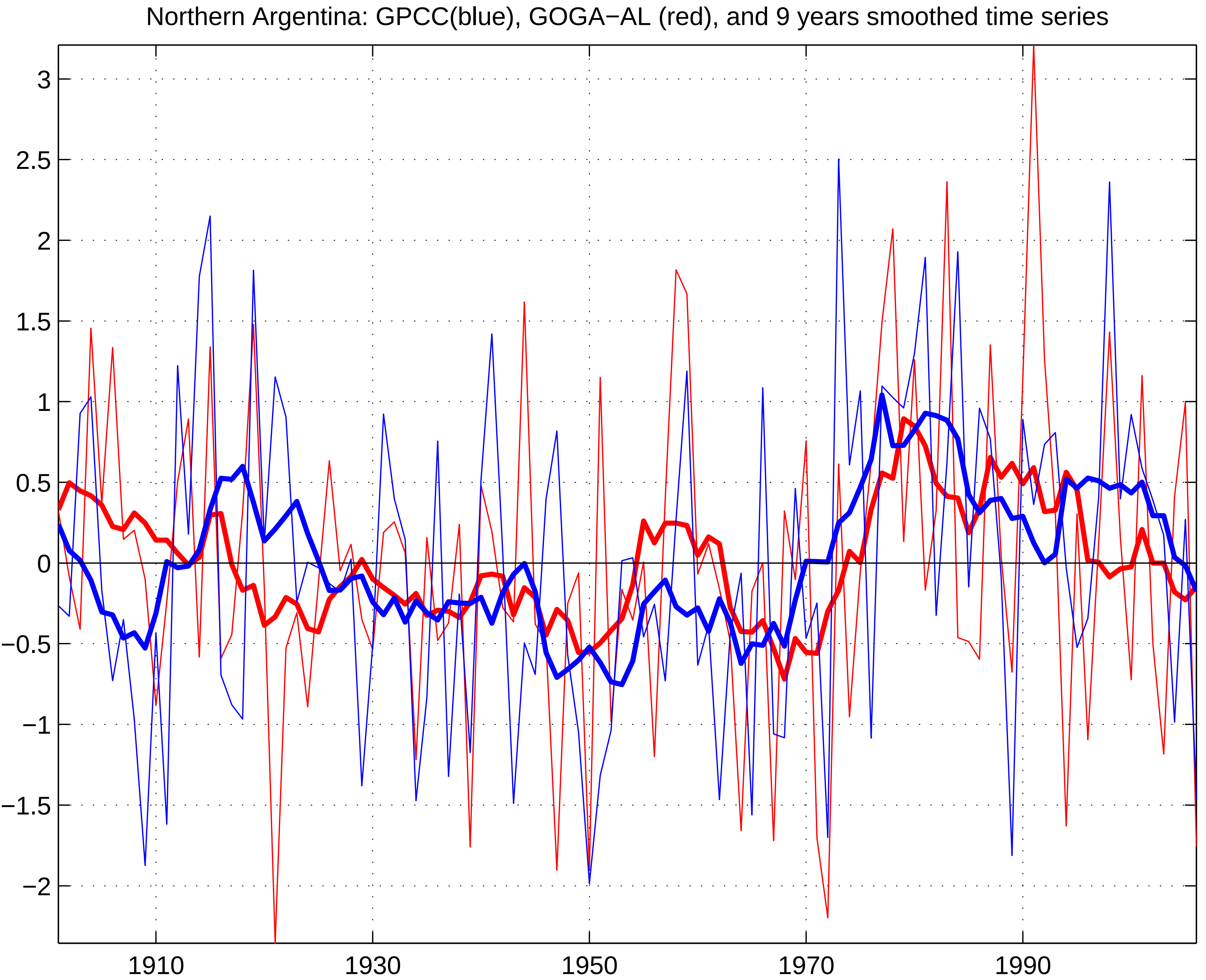
Northern Argentina: GPCC(blue), GOGA−AL (red), and 9 years smoothed time series
3
2.5
2
1.5
1
0.5
0
−0.5
−1
−1.5
−2
1910
1930
1950
1970
1990

Figure 5

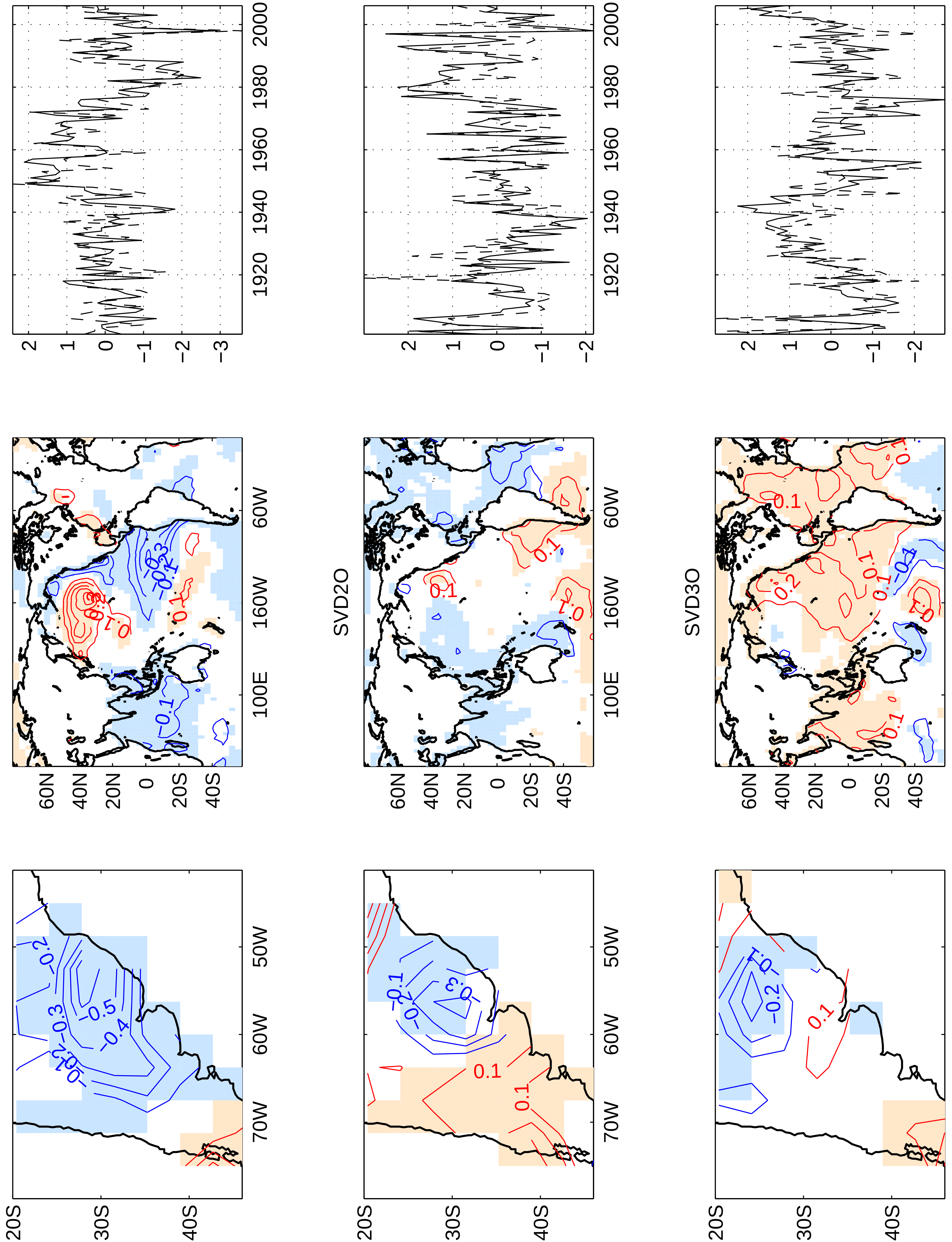

Figure 6

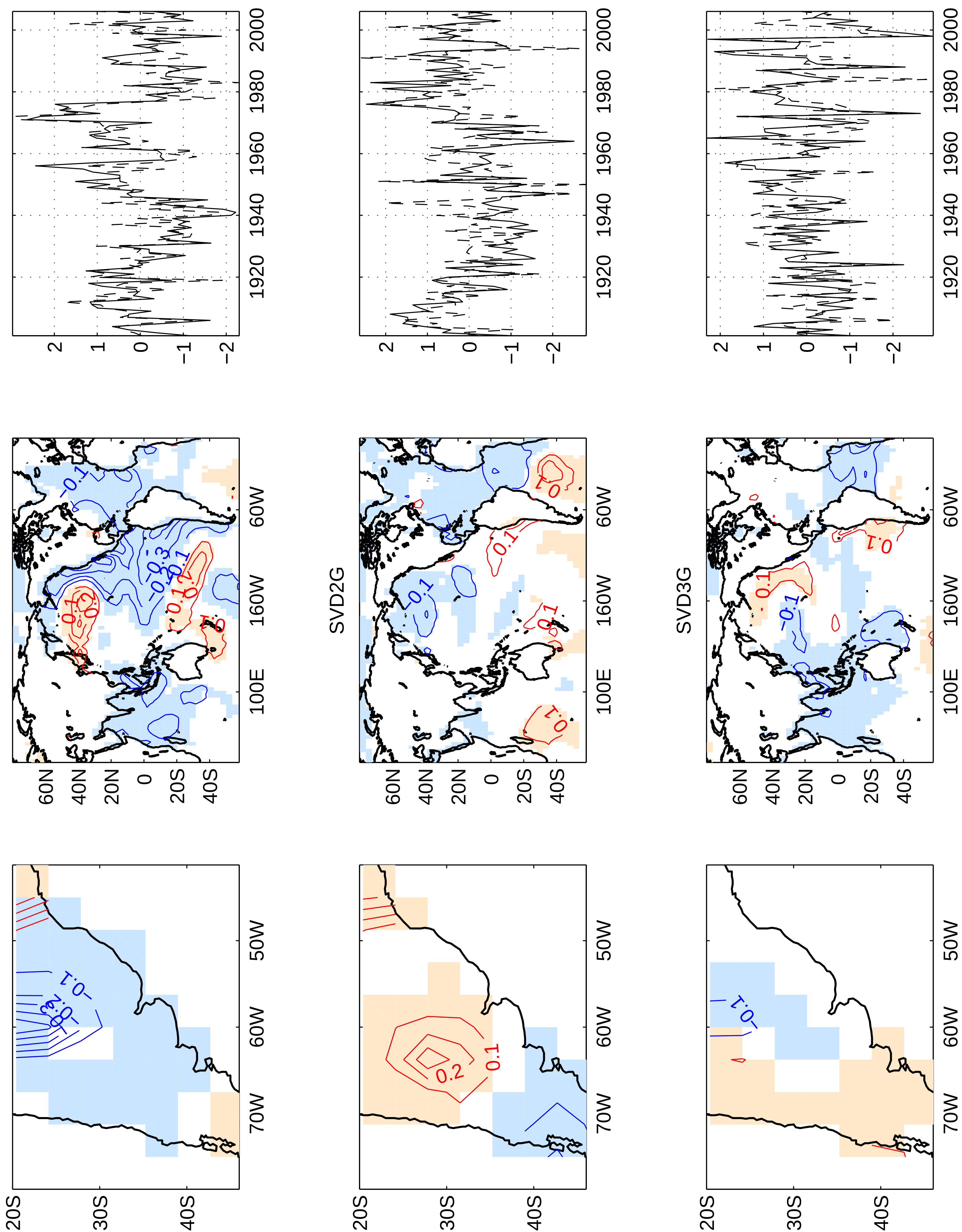
SVD1G
SVD2G
SVD3G
20S
30S
40S
70W
60W
50W
60N
40N
20N
0
20S
40S
100E
160W
60W
2
1
0
−1
−2
1920
1940
1960
1980
2000

Figure 7

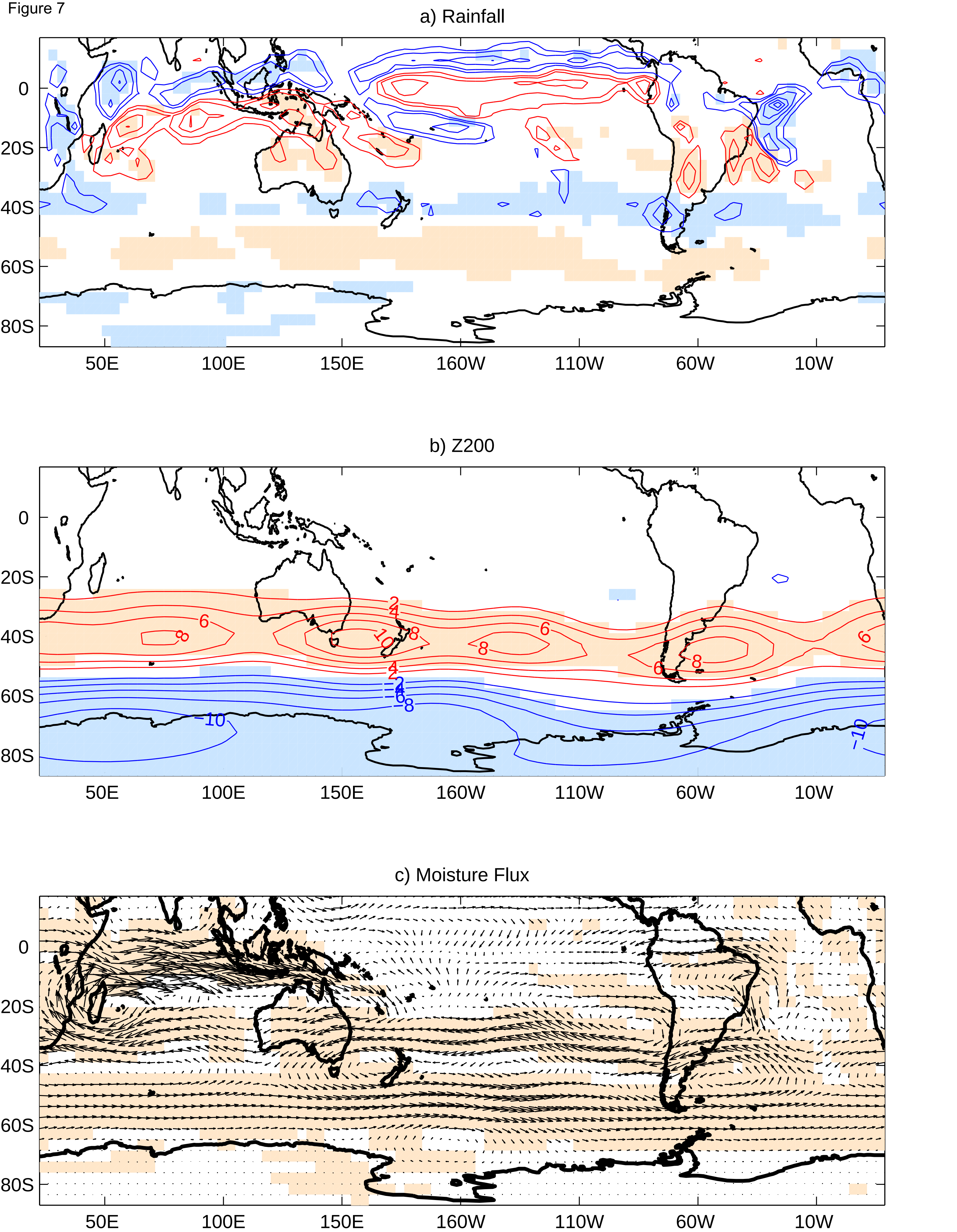

a) Rainfall
b) Z200
c) Moisture Flux
0
20S
40S
60S
80S
50E
100E
150E
160W
110W
60W
10W

Figure 8

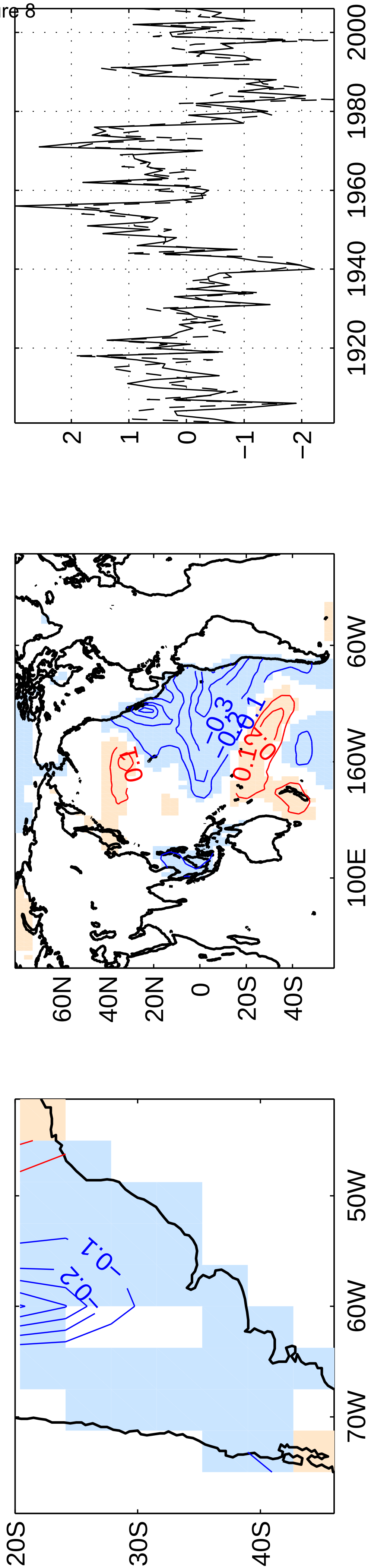

SVD1P
60N
40N
20N
0
20S
40S
100E
160W
60W
-0.3
-0.2
-0.1
0.1
2
1
0
-1
-2
1920
1940
1960
1980
2000
20S
30S
40S
70W
60W
50W
-0.1
-0.2

Figure 9

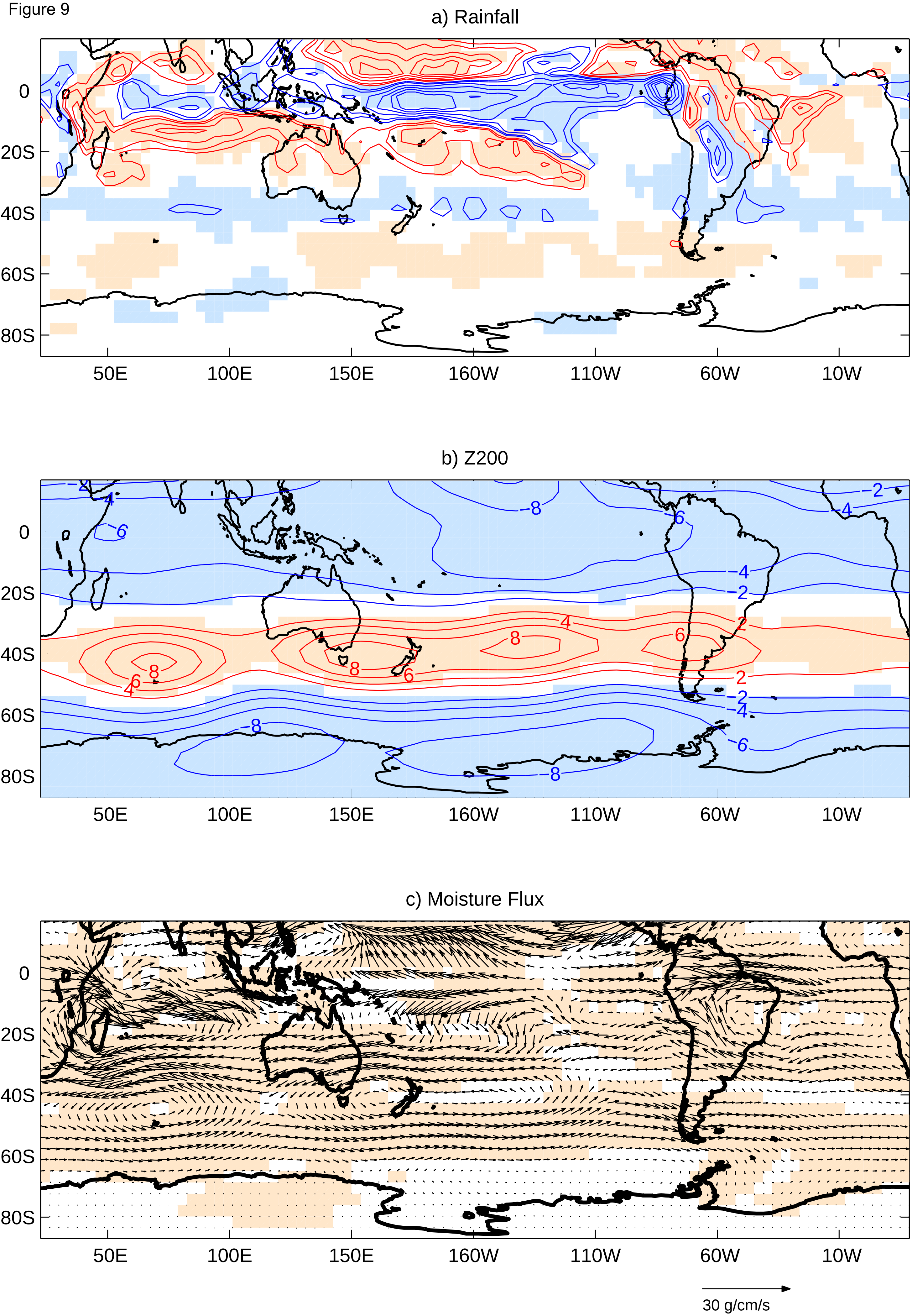
a) Rainfall
0
20S
40S
60S
80S
50E
100E
150E
160W
110W
60W
10W
b) Z200
-2
-4
-6
-8
2
4
6
8
0
20S
40S
60S
80S
50E
100E
150E
160W
110W
60W
10W
c) Moisture Flux
0
20S
40S
60S
80S
50E
100E
150E
160W
110W
60W
10W
30 g/cm/s

Figure 10

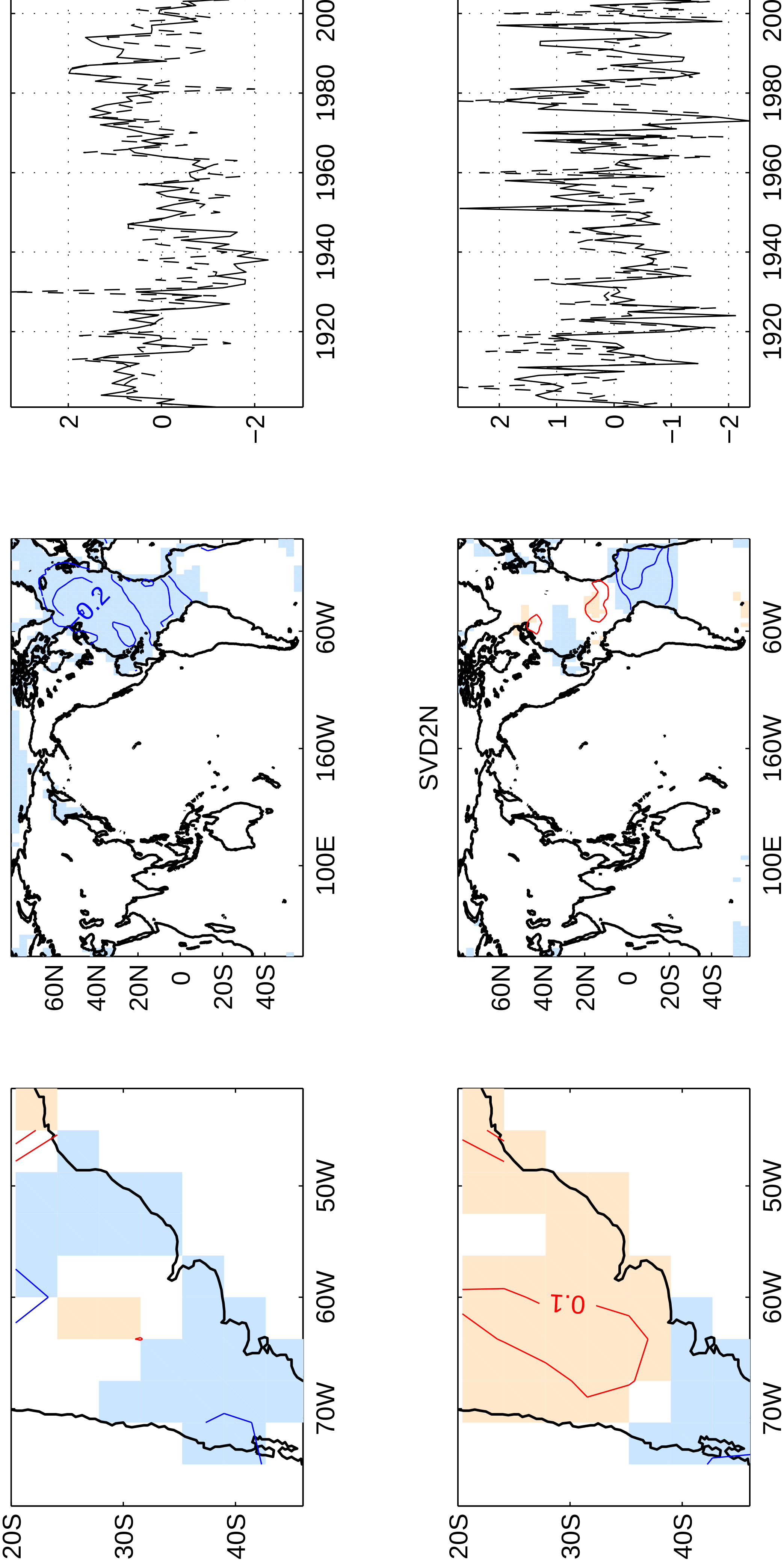
SVD1N
SVD2N
20S
30S
40S
50W
60W
70W
60N
40N
20N
0
20S
40S
100E
160W
60W
-0.2
0.1
2
0
−2
1
−1
1920
1940
1960
1980
2000

Figure 11

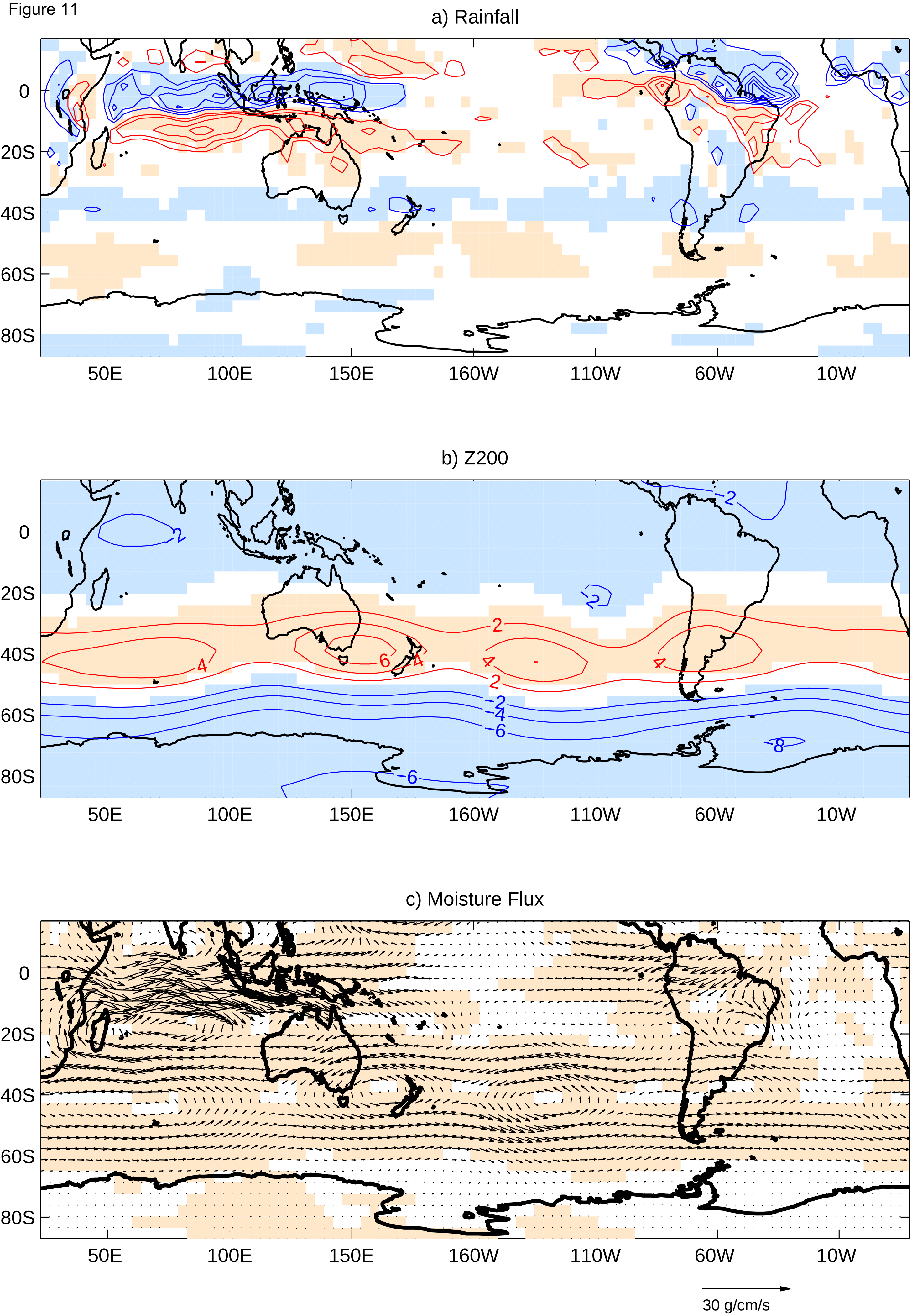
a) Rainfall
b) Z200
c) Moisture Flux
0
20S
40S
60S
80S
50E
100E
150E
160W
110W
60W
10W
30 g/cm/s

Figure 12

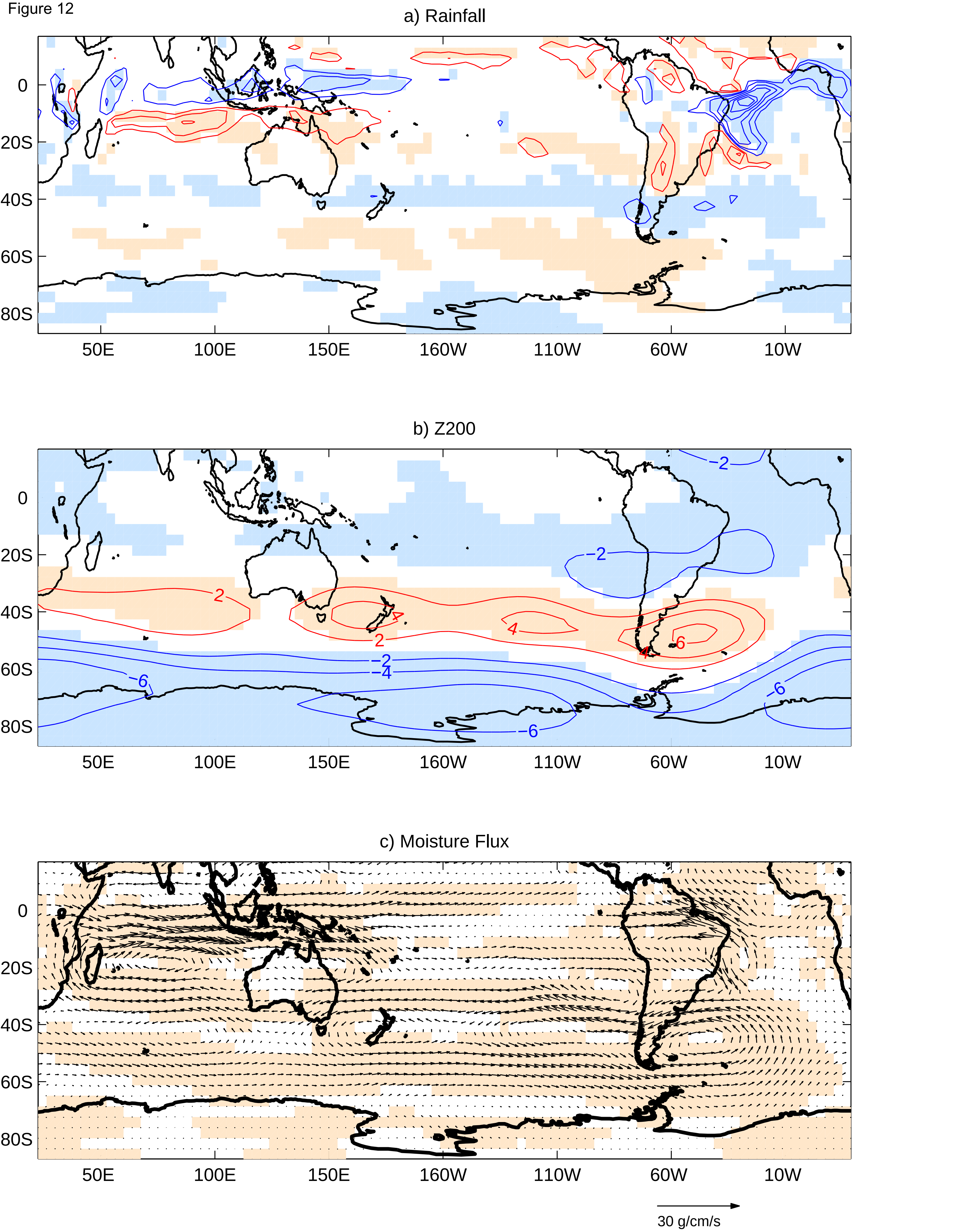

a) Rainfall
b) Z200
c) Moisture Flux
0
20S
40S
60S
80S
50E
100E
150E
160W
110W
60W
10W
-2
2
4
-4
6
-6
30 g/cm/s

Figure 13

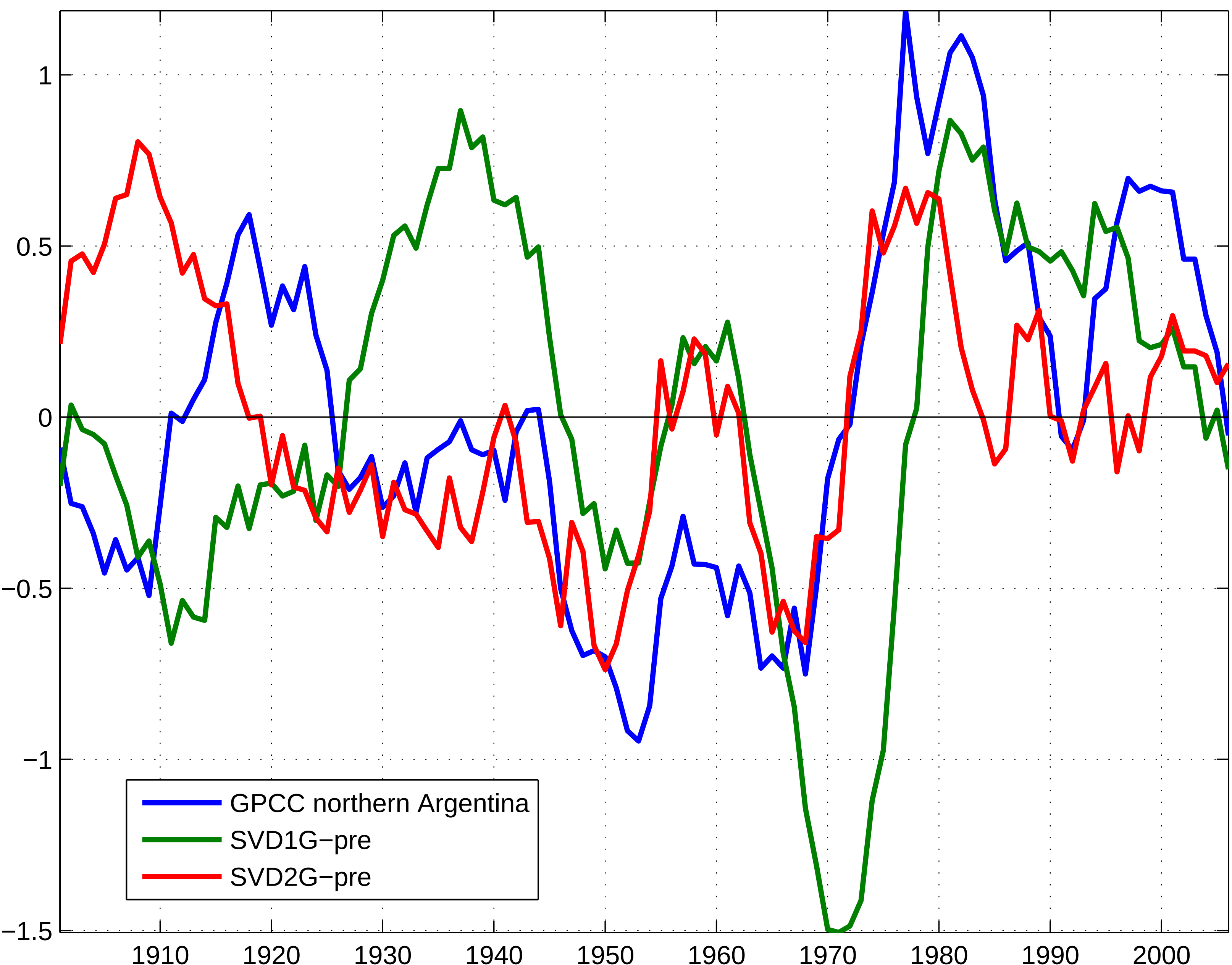

1
0.5
0
−0.5
−1
−1.5
1910
1920
1930
1940
1950
1960
1970
1980
1990
2000
GPCC northern Argentina
SVD1G−pre
SVD2G−pre

Figure 14

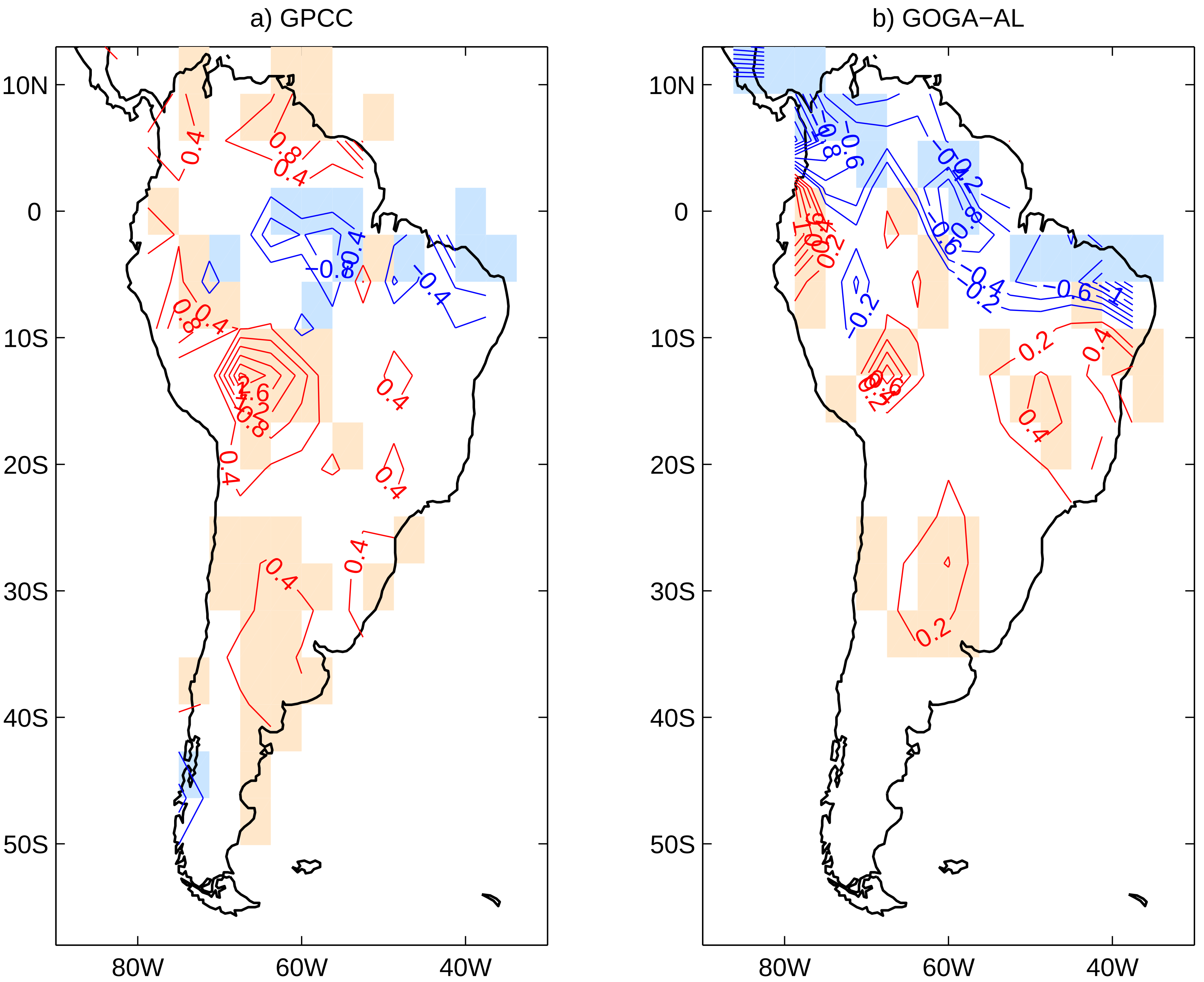

Figure 15

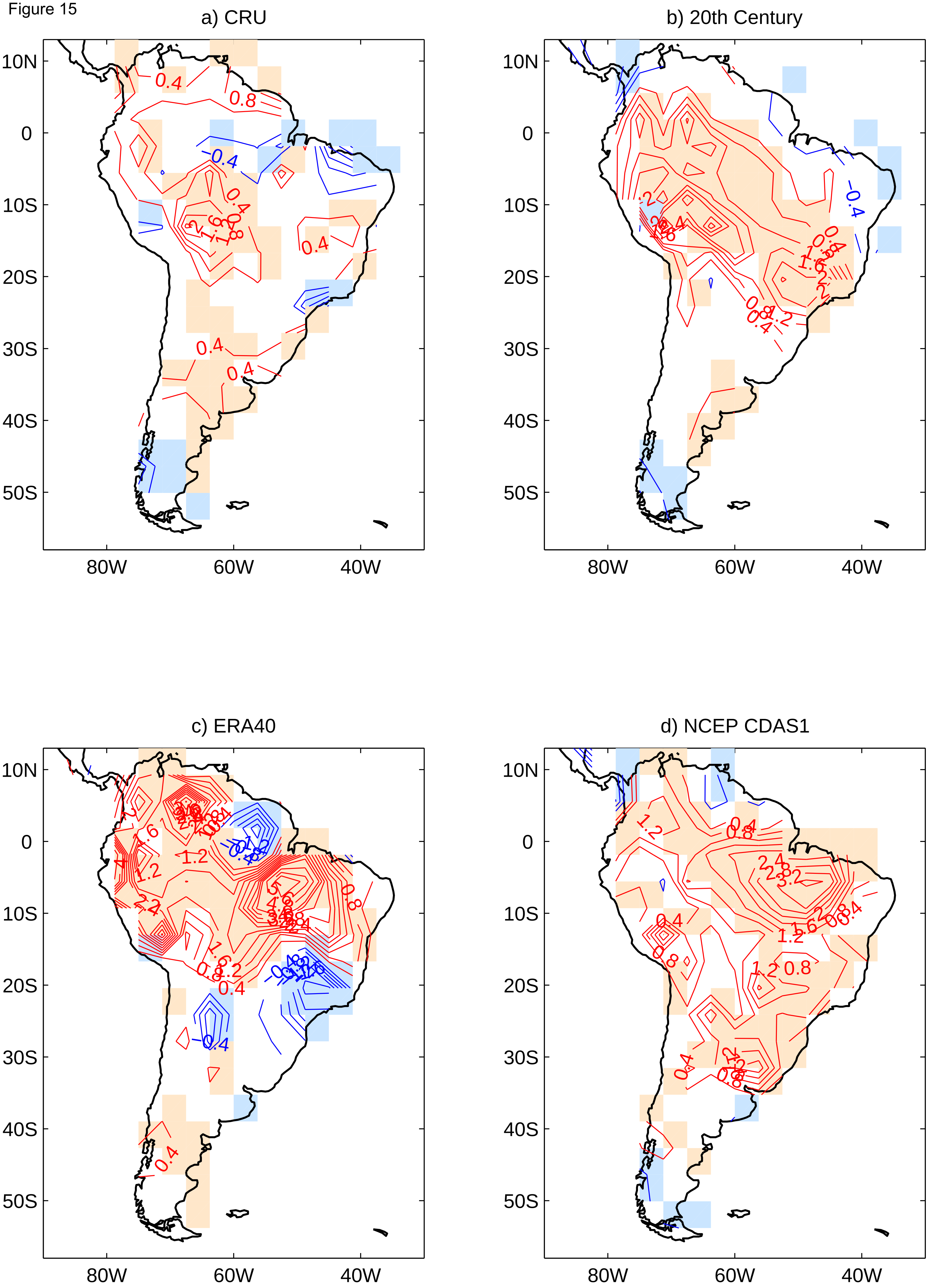
a) CRU
b) 20th Century
c) ERA40
d) NCEP CDAS1
10N
0
10S
20S
30S
40S
50S
80W
60W
40W

Figure 16

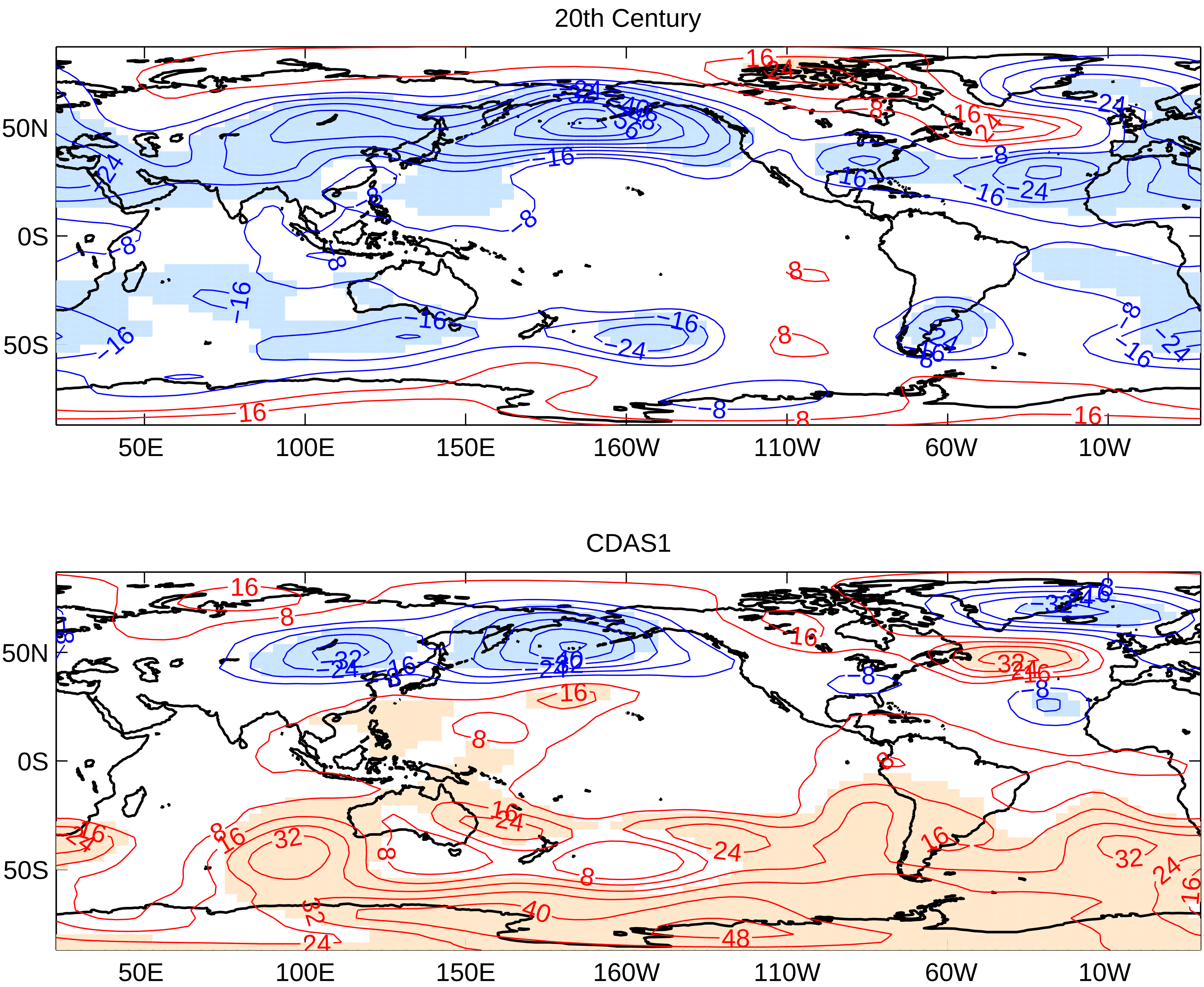
20th Century
50N
0S
50S
50E
100E
150E
160W
110W
60W
10W
CDAS1
50N
0S
50S
50E
100E
150E
160W
110W
60W
10W

Figure 17

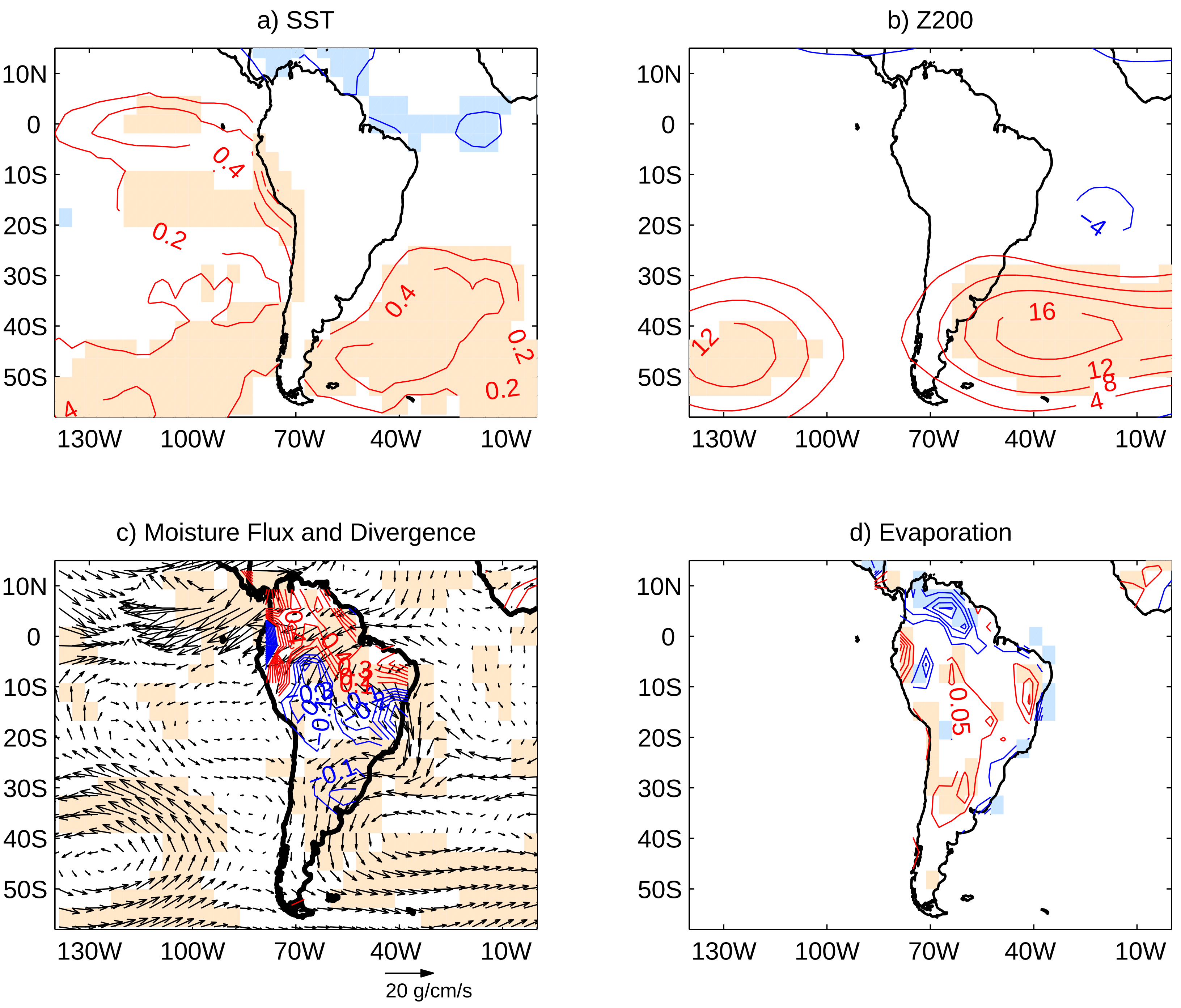

a) SST
b) Z200
c) Moisture Flux and Divergence
d) Evaporation
10N
0
10S
20S
30S
40S
50S
130W
100W
70W
40W
10W
0.4
0.2
16
12
8
4
-4
-0.1
-0.05
20 g/cm/s

Figure 18

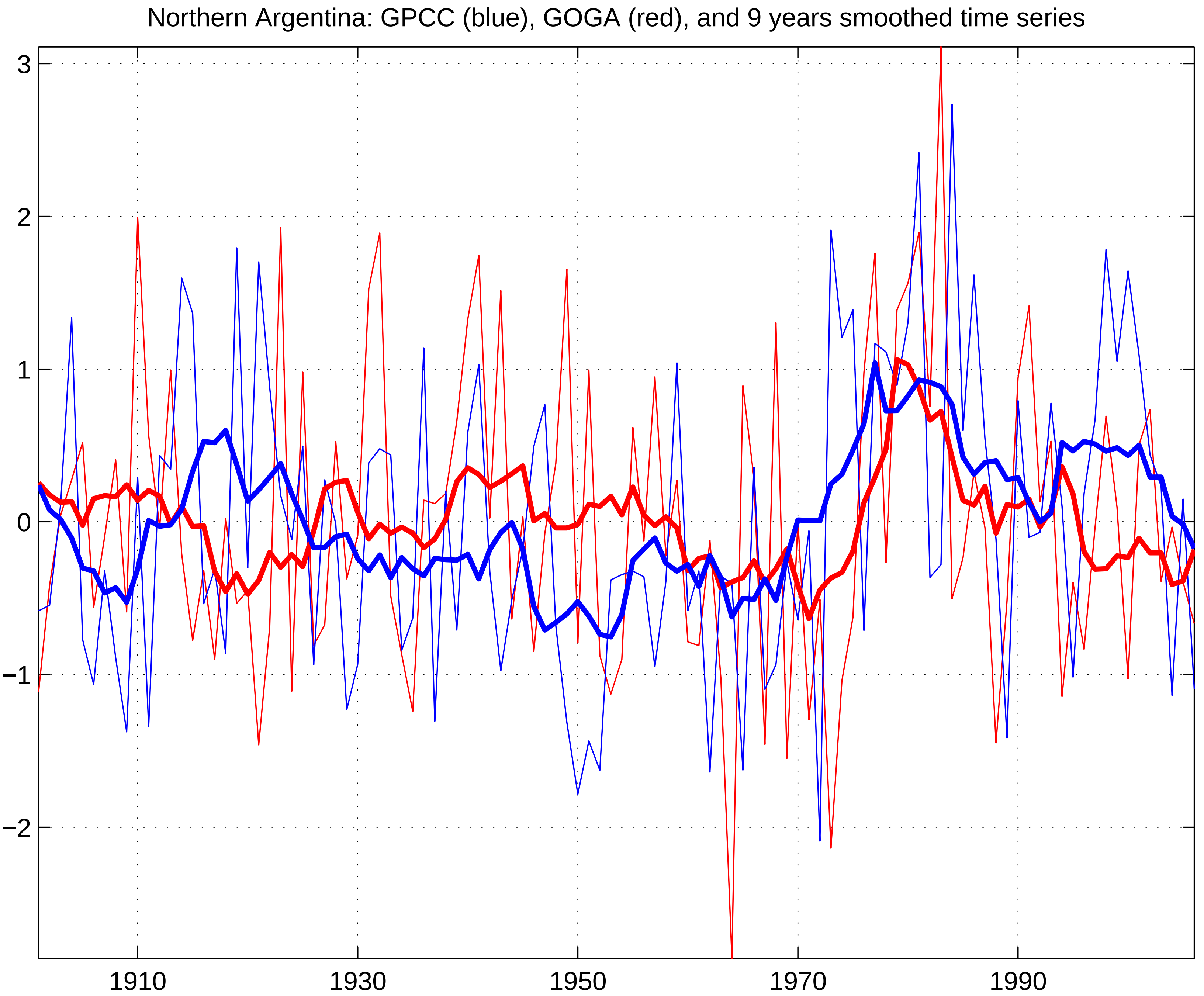
Northern Argentina: GPCC (blue), GOGA (red), and 9 years smoothed time series
3
2
1
0
−1
−2
1910
1930
1950
1970
1990

Figure 19

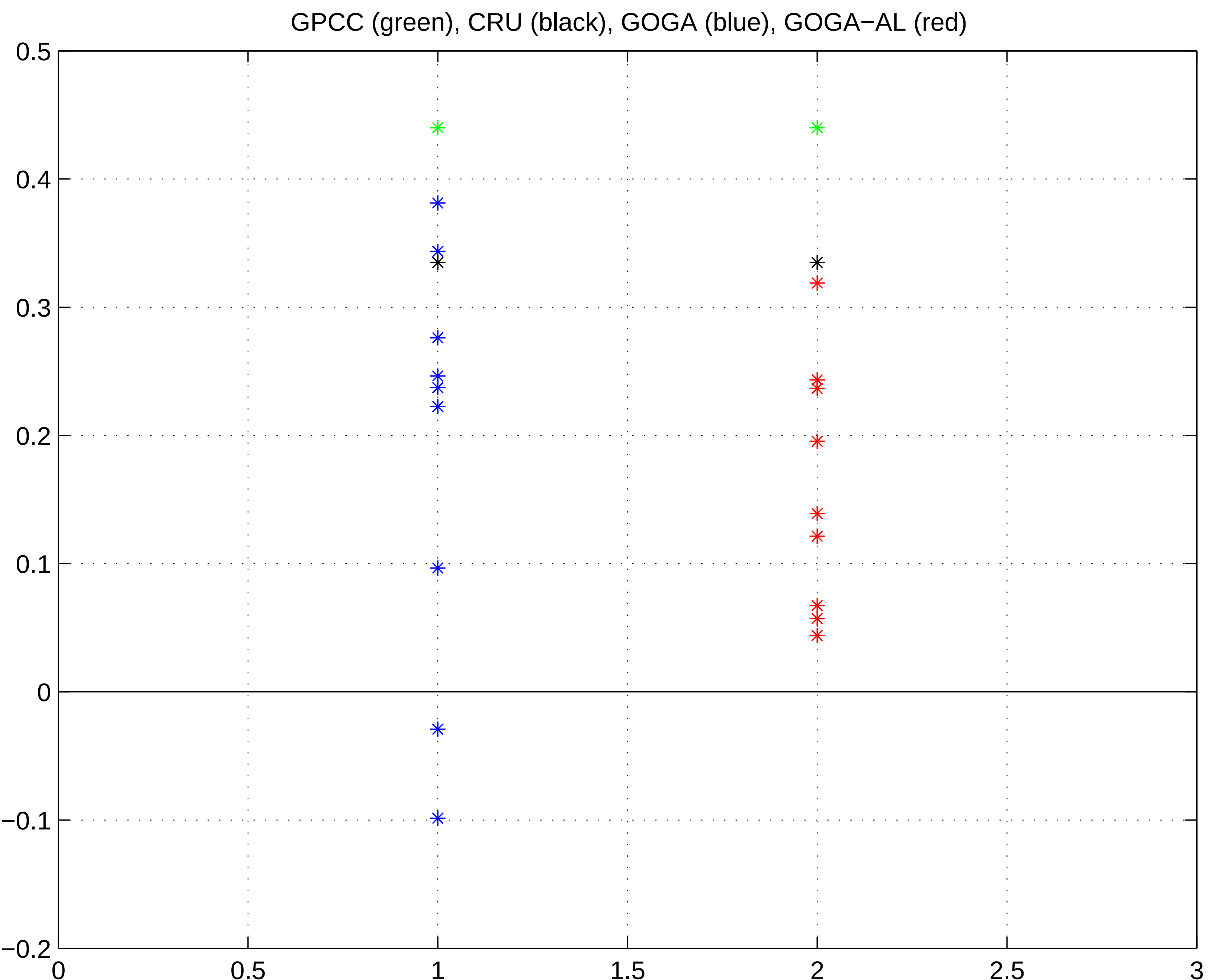
GPCC (green), CRU (black), GOGA (blue), GOGA−AL (red)
0.5
0.4
0.3
0.2
0.1
0
−0.1
−0.2
0
0.5
1
1.5
2
2.5
3